Monthly Notices
of the
ROYAL ASTRONOMICAL SOCIETY

Mon. Not. R. Astron. Soc. **423,** 1351–1367 (2012) doi:10.1111/j.1365-2966.2012.20998.x

The High Time Resolution Universe Pulsar Survey – V. Single-pulse energetics and modulation properties of 315 pulsars

S. Burke-Spolaor[1,2⋆] S. Johnston,[1] M. Bailes,[3,4] S. D. Bates,[5,6] N. D. R. Bhat,[3,4] M. Burgay,[7] D. J. Champion,[8] N. D'Amico,[7] M. J. Keith,[1] M. Kramer,[8] L. Levin,[3] S. Milia,[7,9] A. Possenti,[7] B. Stappers[6] and W. van Straten[3,4]

[1]*Australia Telescope National Facility, CSIRO, PO Box 76, Epping, NSW 1710, Australia*
[2]*NASA Jet Propulsion Laboratory, M/S 138-307, Pasadena, CA 91106, USA*
[3]*Swinburne University of Technology, Centre for Astrophysics and Supercomputing, Mail H30, PO Box 218, VIC 3122, Australia*
[4]*ARC Centre for All-Sky Astronomy (CAASTRO), Australia*
[5]*Department of Physics, West Virginia University, 210E Hodges Hall, Morgantown, WV 26506, USA*
[6]*University of Manchester, Jodrell Bank Centre for Astrophysics, Alan Turing Building, Manchester M13 9PL*
[7]*INAF–Osservatorio Astronomico di Cagliari, localitá Poggio dei Pini, strada 54, I-09012 Capoterra, Italy*
[8]*Max Planck Institut für Radioastronomie, Auf dem Hügel 69, 53121 Bonn, Germany*
[9]*Dipartimento di Fisica, Universitá degli Studi di Cagliari, Cittadella Universitaria, 09042 Monserrato (CA), Italy*

Accepted 2012 March 19. Received 2012 March 15; in original form 2012 January 23

ABSTRACT

We report on the pulse-to-pulse energy distributions and phase-resolved modulation properties for catalogued pulsars in the southern High Time Resolution Universe intermediate-latitude survey. We selected the 315 pulsars detected in a single-pulse search of this survey, allowing a large sample unbiased regarding any rotational parameters of neutron stars. We found that the energy distribution of many pulsars is well described by a log-normal distribution, with few deviating from a small range in log-normal scale and location parameters. Some pulsars exhibited multiple energy states corresponding to mode changes, and implying that some observed 'nulling' may actually be a mode-change effect. PSR J1900−2600 was found to emit weakly in its previously identified 'null' state. We found evidence for another state-change effect in two pulsars, which show bimodality in their *nulling time-scales*; that is, they switch between a continuous-emission state and a single-pulse-emitting state. Large modulation occurs in many pulsars across the full integrated profile, with increased sporadic bursts at leading and trailing sub-beam edges. Some of these high-energy outbursts may indicate the presence of 'giant pulse' phenomena. We found no correlation with modulation and pulsar period, age or other parameters. Finally, the deviation of integrated pulse energy from its average value was generally quite small, despite the significant phase-resolved modulation in some pulsars; we interpret this as tenuous evidence of energy regulation between distinct pulsar sub-beams.

Key words: astronomical databases: miscellaneous – pulsars general.

1 INTRODUCTION

Radio pulsars have long been known to display a myriad of intrinsic amplitude modulation effects. Averaged over many rotations, most pulsars have a reproducible pulse shape, reflective of the long-term stability of their rotation and magnetism. In contrast, sequential rotations of a pulsar can differ considerably in pulse shape and intensity; ordered effects such as subpulse drift, mode changing and nulling (e.g. Backer 1970; Cole 1970), as well as stochastic pulse-to-pulse shape and intensity variations affect pulsars to varying degrees. Other effects such as intense giant pulses (Staelin & Reifenstein 1968; Comella et al. 1969) or 'giant micropulses' (referencing their narrow structure; e.g. Johnston et al. 2001) occur in some pulsars at a limited phase range.

The energy distribution of radio pulses can provide a window into the state of pulsar plasma and the method of emission generation. There exist a great number of viable plasma-state models, a few of which predict pulse energy distributions; the most commonly proposed predictions are of Gaussian, log-normal and power-law

⋆E-mail: sarah.burke-spolaor@jpl.nasa.gov

distributions. Cairns, Johnston & Das (2003a) and Cairns et al. (2003b), and references therein, provide discussion on these models. Energy distributions have been examined in detail for only a few pulsars (Cognard et al. 1996; Cairns, Johnston & Das 2001, 2004), resulting in the conclusion that those pulsars obey log-normal statistics. These analyses have substantially contributed to the hypothesis that genuine 'giant pulses' are generated separately from standard pulse generation; while 'giant pulse' is sometimes used to refer to any single pulse of more than 10 times the average intensity, studies have revealed giant pulses with power-law energy distributions, distinct from log-normal main pulse components (Lundgren et al. 1995; Johnston & Romani 2002; Kramer, Johnston & van Straten 2002). No survey targeting single-pulse energy distribution shapes or giant pulses in the general population has yet been performed.

Phase-resolved modulation analysis is likewise thought to be an indicator of radio emission's geometry and generation mechanism. Weisberg et al. (1986) first noted differences in modulation between core and conal-type pulse profiles, while Jenet & Gil (2003) derived theoretical predictions for anticorrelations between the modulation index (defined in Section 3.4) and four 'complexity parameters', corresponding to four pulsar emission models. Their complexity parameters are $a_1 = 5\dot{P}^{2/6}P^{-9/14}$, for the sparking gap model, $a_2 = (\dot{P}/P^3)^{0.5}$ for the continuous current outflow instabilities, $a_3 = (P\dot{P})^{0.5}$ for surface magnetohydrodynamic wave instabilities and $a_4 = (\dot{P}/P^5)^{0.5}$ for outer magnetospheric instabilities. The Jenet & Gil (2003) measurements of modulation index for a small sample of core-type profiles disfavoured the magnetohydrodynamic wave instability model. The studies of Weltevrede, Edwards & Stappers (2006a) and Weltevrede, Stappers & Edwards (2007) surveyed ordered, longitude-resolved modulation in ∼190 pulsars at 21 and 92 cm. Their large sample enabled them to test correlations with other neutron star properties. They determined that the modulation index is generally higher at lower frequencies, and noted a weak correlation between modulation index and age that is dampened at higher frequency.

The study of single-pulse modulation in a large pulsar sample can also contribute to several practical questions: for instance, how common is giant-pulse emission, and are some 'giant pulses' the manifestation of a broad log-normal energy distribution? Are the prospects of pulsar detection in other galaxies better for single-pulse or Fourier searches (e.g. Johnston & Romani 2003; McLaughlin & Cordes 2003)? Quantification of pulsars' modulation will also aid in understanding the physical makeup of 'rotating radio transients' (RRATs; McLaughlin et al. 2006). Energy distributions in bright, individual RRATs show that some appear to be pulsars with extremely high (≫95 per cent) nulling fractions (e.g. Burke-Spolaor & Bailes 2010; Burke-Spolaor et al. 2011; Miller et al. 2011). However, an unknown fraction of RRATs may be distant pulsars with extremely broad energy distributions, such that only their brightest, infrequent pulses are detectable (Weltevrede et al. 2006b). The distinction between these two cases will be critical in quantifying RRATs' potentially overwhelming contribution to Galactic pulsar populations (Keane & Kramer 2008); however, the general pulsar population's intrinsic energy distributions have not yet been extensively studied.

The High Time Resolution Universe survey recently completed its southern intermediate-latitude ('HTRU med-lat') survey of Galactic latitudes $|b| < 15^\circ$ and longitudes $-120^\circ < l < 30^\circ$ for pulsars (Keith et al. 2010) and single pulses (Burke-Spolaor et al. 2011). Single pulses from known pulsars were detected at rates that vastly improve on previous surveys of the same region, testifying to the increased sensitivity of the high dynamic range, frequency resolution and time resolution of a new digital search back-end on Parkes radio telescope (described in Keith et al. 2010).

In this paper, we study the modulation properties of all med-lat pulsars with detectable single pulses, using the relatively unbiased, single-pulse flux-limited sample provided by the HTRU med-lat survey. We focus here on studies that can be performed within the survey's 9-min observations, pursuing pulse intensity distribution statistics and the measurement of basic pulse-to-pulse modulation properties. In Section 2 we describe our sample selection, and Section 3 describes our analysis methods. In Sections 4 and 5, we describe the results of our energy distribution analysis and modulation analysis, respectively, and provide discussion of the results. Section 6 reviews other science aspects addressed by our analysis. Section 7 summarizes our findings.

2 DATA AND PULSAR SAMPLE

Our data are made up of HTRU med-lat survey observations. This survey had 64-μs sampling, and a bandwidth of 340 MHz is divided into 870 frequency channels, centred on 1352 MHz. Two polarization channels are summed prior to data recording, and data are digitized using 2 bits. The system temperature was 23 K.

2.1 Determination of pulsar sample

The initial pulsar set included all pulsars in the med-lat survey region as queried through the online ATNF Pulsar Database (PSRCAT).[1] We selected the observation of smallest angular distance within 0.°25 to each pulsar, yielding 1159 observations near 1113 pulsars (some had multiple observations at roughly equal distance to the pulsar). We scrutinized the HTRU Fourier and single-pulse search results for each observation (as described in Keith et al. 2010 and Burke-Spolaor et al. 2011, respectively) to determine the pulsar's detectability. Single pulses were 'detected' if a pulse peaking near the pulsar's dispersion measure (DM) exceeded a significance of 6, and was confirmed by inspection of the data. 411 pulsars were not detected by single-pulse or Fourier analysis,[2] and 16 were detected only through single-pulse analysis. Of the Fourier-detected pulsars, 45 per cent had at least one detected single pulse. It is the 315 pulsars with detected single pulses that we analyse in this study.

Our sample is not isolated in period–period derivative phase space, consistent with previous studies (e.g. Burke-Spolaor & Bailes 2010). We explore the full range of pulsars' magnetic field strength (B), energy derivative ($\dot{E}$), period (P), period derivative ($\dot{P}$) and characteristic age (τ_c), giving us acute sensitivity to any dependence of modulation effects on these parameters. Our sample includes two millisecond pulsars (PSRs J1439−5501 and J1744−1134) and one radio magnetar (PSR J1622−4950; Levin et al. 2010).

2.2 Pulse stacks and data configuration

We dedispersed each observation and resampled the resulting time series to break it into integrations of duration equal to the pulsar's rotational period. We used DMs and periods as predicted by PSRCAT

[1] Originally published by Manchester et al. (2005), available at http://www.atnf.csiro.au/research/pulsar/psrcat/.

[2] These non-detections were investigated, and typically found to be due to strong interference, scintillation or insufficient integration time (i.e. the faint objects discovered by the 35-min Parkes multibeam survey pointings; Manchester et al. 2001).

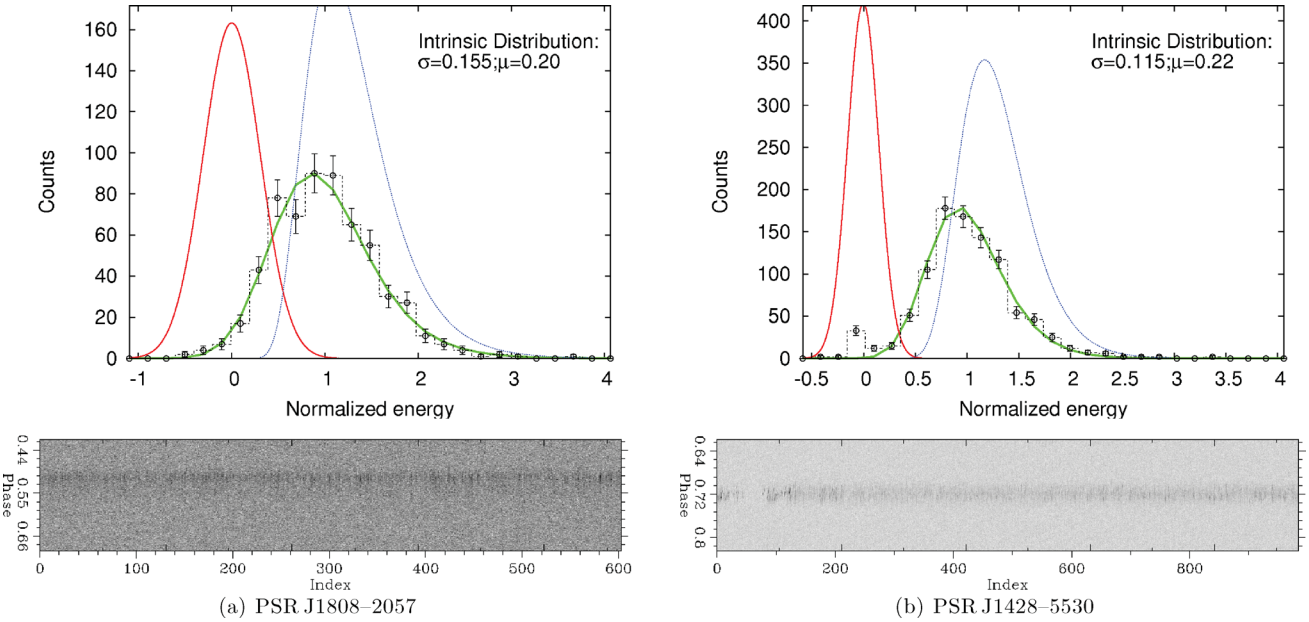

(a) PSR J1808–2057 (b) PSR J1428–5530

Figure 1. Two examples of pulsars with log-normal energy distributions. The upper plots show the energy distribution of on-pulse data (black dash–dotted histogram with points and error bars), the log-normal energy model fits (thick green line), the off-pulse noise model (thin red line) and the intrinsic energy distribution (blue dotted line). Errors shown are the square root of the number in each bin. The lower plots show the corresponding pulse stacks for each pulsar. PSR J1428−5530, in (b), has a brief nulling episode from pulse indexes ∼50–80 that is visible, distinct from the log-normal distribution for non-null pulses. A figure showing all pulse stacks, energy distributions and phase-resolved modulation is available online (see Supporting Information, Appendix A).

ephemerides. In some cases, the observed period did not match the ephemeris prediction. For these we used the rotational period measured in our observation. Each integration consisted of 1024 phase bins, or in some cases integer divisors of two where needed to ensure the size of one bin equalled or exceeded the sampling time of the original data. This caused slightly degraded longitude resolution for short-period pulsars.

Throughout this analysis we refer to 'pulse stacks', which are the observed power represented as a function of pulse phase and number (indexed from the observation's start), as shown in the lower panels of Fig. 1.

3 METHODS AND ANALYSIS

3.1 Flux and energy measurements

Normalized energy, $E/\langle E\rangle$, was calculated using the standard method for determining pulse energy distributions (e.g. Ritchings 1976; Biggs 1992). In each observation, we defined on-pulse windows of size $N_{\rm on}$ bins, the position and width of which were determined by inspection of the integrated pulsar profile. Where the pulsar duty cycle was less than 0.5, we chose an off-window also of size $N_{\rm on}$ to determine the off-pulse energy. All bins not part of the on-window were used to estimate the integration's per-bin standard deviation, and to remove a baseline from all bins. We did not divide integrations into shorter analysis blocks (as in Ritchings 1976), as interstellar scintillation at our observing frequency for each pulsar was expected, and observed, to be minimal based on the NE2001 Galactic electron density and scintillation model (Cordes & Lazio 2002). Furthermore, it was realized that block analysis mutes the modulation induced by intermediate-time-scale nulling and mode changing in some pulsars. The normalized on-pulse and off-pulse energies ($E_{\rm on}$ and $E_{\rm off}$, respectively) were calculated for each stellar rotation by integrating the energy in the on- and off-window bins, respectively, then dividing by the mean on-pulse energy of all integrations. The single-pulse energy significance, $\langle s_{\rm E}\rangle$, is given by $\langle s_{\rm E}\rangle = E_{\rm on}/(\sigma\sqrt{N_{\rm on}})$, where σ is the standard deviation of the off-pulse energy.

3.2 Energy distribution tests

We performed analysis of pulse energy distributions to assess whether the probability distribution function of pulse energy is well fitted to either a log-normal or Gaussian distribution, and if so, whether pulsars share typical distribution parameters. We analysed the $E_{\rm on}$ distributions by constructing histograms of $E_{\rm on}$ and $E_{\rm off}$ in 25 fixed-size bins over the full range of detected normalized energy for each available observation. We modelled each observation's noise with a Gaussian of the same mean and standard deviation as the off-pulse distribution.

We then performed a least-squares minimization of the data fitted by a model for the intrinsic on-pulse energy distribution convolved with noise. The test distributions were defined by Gaussian and log-normal probability density functions. For the Gaussian case, we tested a grid of probable values in the range $0.02 < \sigma_{\rm g} < 1.10, 0.2 < \mu_{\rm g} < 4.0$, where $\sigma_{\rm g}$ and $\mu_{\rm g}$ are the standard deviation and mean of the distribution, respectively. In the log-normal case, we tested over scale and location parameters in the range $0.02 < \sigma_\ell < 1.10, -2.0 < \mu_\ell < 2.0$, where these parameters are defined in the probability distribution as

$$P(E) = \frac{1}{E\sigma_\ell\sqrt{2\pi}}\exp\left[\frac{-(\log_{10}(E)-\mu_\ell)}{2\sigma_\ell^2}\right]. \quad (1)$$

We sampled each test distribution at equal bin size and range as the data, then convolved it with the Gaussian noise model. A

least-squares fit was then computed between the noise-convolved model and the data.

The goodness of fit of the best-fitting distribution was quantified by a χ^2 analysis, using only bins where the value of the convolved model in the bin was greater than 5.[3] We took the degrees of freedom to be the number of valid bins minus 3, and a goodness-of-fit probability was calculated from the χ^2 cumulative distribution function and the fit's χ^2 value. Probabilities were calculated for both the logarithmic and Gaussian cases (giving P_ℓ and P_g, respectively). Finally, the best-fitting convolved Gaussian and log-normal models were overlaid on the data (e.g. Fig. 1) and inspected by eye to aid in classification of the energy distributions. The results of this analysis are described and discussed in Section 4.

3.3 Recognition of pulse nulling

We performed an inspection of both pulse stacks and pulse energy distributions to determine whether nulls were either not present, or clearly present, in each observation. In Table 1, we indicate for each pulsar whether no null pulses were observed (marked by N, indicating no pulses occurred at a zero energy state), or whether a peak at zero energy was discernible from a distinct on-pulse distribution (marked by Y). For the remaining pulsars, we could not distinguish the presence or non-presence of nulls without further analysis, which will be performed in the future for all pulsars observed in the HTRU med-lat survey. We could distinguish 31 pulsars (∼10 per cent of the full sample) with no observed nulls and 69 pulsars (∼22 per cent of the sample) with a null state. The remaining pulsars in the sample were not sufficiently bright to distinguish whether they were nulling or not.

3.4 Parametrization of modulation

We quantified the longitude-resolved modulation in each pulsar by computing two values for each bin of a pulse stack. The observed 'modulation index' is defined as $m_{\mathrm{obs},j} = \sigma_j/\mu_j$, where σ_j and μ_j are the standard deviation and the mean across the whole observation, respectively, of the jth bin. Interstellar scintillation can induce signal in $m_{\mathrm{obs},j}$ of $m_{\mathrm{ISM}} = (1 + \eta B/\delta b)^{-1/2}$, where $B = 340$ MHz is the receiver bandwidth, η is a filling factor and δb is the scintillation bandwidth of the pulsar. We determined δb from the Cordes & Lazio (2002) Galactic electron density model and scaled the value to the centre HTRU survey observing frequency of 1.352 GHz assuming $\delta b \propto f^4$. The induced m_{ISM} value was inferred using the prescription of Jenet & Gil (2003), where setting $\eta = 0.18$, the intrinsic modulation index is

$$m = \left(\frac{m_{\mathrm{obs}}^2 - m_{\mathrm{ISM}}^2}{m_{\mathrm{ISM}}^2 + 1} \right)^{1/2}. \quad (2)$$

The modulation index is most sensitive to persistent oscillations in a pulsar's signal, e.g. as would be caused by subpulse drift or mode changing on time-scales much less than the observation time. This parameter has poor accuracy for observations of low integrated signal-to-noise ratio (S/N), for instance it is undefined off-pulse, and is insensitive to non-persistent modulation like sporadic or infrequent outbursts.

To identify sparse modulated emission (on- and off-pulse), we use the R modulation statistic introduced by Johnston et al. (2001). They define the R-parameter as $R_j = (M_j - \mu_j)/\sigma_j$, again computed in the jth bin of each observation, where M_j is the maximum value observed in that bin. Given that the per-bin statistics are (in the absence of pulsar signal or interference) Gaussian-distributed, even off-pulse regions are expected to exhibit R_j values consistent with a Gaussian distribution. This and its dependence on the significance of mean single-pulse brightness render it difficult to use as an absolute comparative modulation statistic between pulsars; however, it is ideal for identifying the presence of giant pulses, and other extreme phase-dependent, sparse modulation or significantly non-Gaussian behaviour. We consider a measurement of R_j 'significant' if the bin's value minus the off-pulse mean is more than four times the standard deviation of the R_j values in the off-pulse window.

4 SINGLE-PULSE ENERGY DISTRIBUTIONS

Here we describe the results of our energy distribution fitting analysis, with the goal of characterizing the field statistics of the radio-generating pulsar plasma. Section 4.1 organizes the pulsars into categories defined by their energy distribution shape. Section 4.2 interprets these class divisions in terms of underlying pulsar energy statistics, taking into account the noise properties of our data and other caveats of the fitting analysis. That section also reviews the typical distribution parameters defining the best-fitting pulsar shapes. Finally, Section 4.3 explores the cause of the distinct, multiple, non-zero energy peaks exhibited by some pulsars in our sample.

4.1 Classification of energy distributions

Table 1 reports our classifications (described below) for each pulsar, along with the best-fitting parameters and goodness-of-fit probability for the Gaussian and log-normal fits.

During visual inspection of the energy distributions, we noted multiple non-null peaks in the distributions of some pulsars. As with nulling pulsars, these are not unimodal and thus their best-fitting distribution statistics are not reliable. We provide the fit results in Table 1 for nulling and multipeaked pulsars only for the sake of Section 4.2 discussion. Several nulling pulsars had a sufficiently bright non-null state to have a recognizably distinct distribution from the null pulses. These are identifiable in Table 1 as pulsars with a distribution class (column 9) reported in parentheses. An example of such a case is shown in Fig. 1(b). These objects are included in our statistical analyses. Multipeaked energy distributions were defined as any distribution with either more than two points deviating more than one standard deviation, or one point deviating more than two standard deviations from a smooth single-peaked distribution. These were identified by inspection of the pulse energy plots.

We divided the pulsars into five energy distribution classifications (the percentage of constituent pulsars is given for each category; these percentages are calculated based on the 255 non-nulling, and classifiable-nulling, pulsars).

(i) *Log-normal (L; 33 per cent).* Distribution appeared unimodal and the best-fitting results obeyed $P_\ell \geq 0.75$ and $P_g < 0.75$.

(ii) *Gaussian (G; 3 per cent).* Distribution appeared unimodal and the best-fitting results obeyed $P_\ell < 0.75$ and $P_g \geq 0.75$.

(iii) *Unimodal (U; 9 per cent).* P_ℓ and P_g were $\geq$0.75.

[3] Note that the χ^2 value we use is defined using $\chi^2 = \sum[(\text{data value} - \text{model value})^2/(\text{model value})]$, which avoids the use of ill-defined errors on our distributions. This is not expected to introduce a bias in the measured goodness-of-fit probability or distribution parameters because the initial fit was performed using a least-squares minimization that took the full distribution into account.

Table 1. The numerical results of the energy distribution and modulation analysis. Columns are (1) PSR name (J2000); (2) number of pulses detected in blind single-pulse search, and total number of rotations in the observation; (3) integrated (Fourier) S/N; (4) S/N of the brightest single pulse detected in the blind single-pulse search; (5) average single-pulse energy significance; (6) maximum R_j value, where significant; (7) minimum on-pulse, phase-resolved modulation index, where significant; (8) indication of whether pulse appears to be nulling (Y) or had no zero-energy pulses (N); (9) energy distribution classification; (10–12) the probability and fit values associated with the best-fitting log-normal energy distribution; (13–15) the probability and fit values associated with the best-fitting Gaussian energy distribution.

(1) PSR Jname	(2) Npulses	(3) S/N (int)	(4) S/N (SP)	(5) $\langle s_E \rangle$	(6) Max. R_j	(7) Min. m_j	(8) Null?	(9) Dist. class	(10) P_ℓ	(11) σ_ℓ	(12) μ_ℓ	(13) P_g	(14) σ_g	(15) μ_g
J0726−2612	17/163	18.4	35.4	1.2	9.3	–	Y	–	0.2363	0.05	1.02	0.0023	0.30	2.86
J0738−4042	1469/1482	2645.5	47.1	53.3	11.1	0.3523	N	G	0.1387	0.07	0.12	0.7804	0.21	1.15
J0742−2822	3306/3341	1303.5	35.4	19.9	6.3	0.3353	N	O	0.0119	0.07	0.10	0.0000	0.18	1.10
J0745−5353	126/2625	163.6	15.6	2.7	5.5	1.8748	–	O	0.0017	0.10	0.27	0.0000	0.30	1.34
J0809−4753	12/1024	101.8	8.0	2.7	–	1.0487	–	L	0.9372	0.09	0.15	0.2798	0.24	1.20
J0818−3232	49/251	64.1	13.7	2.9	5.6	–	–	L	0.9289	0.17	0.17	0.1499	0.44	1.20
J0820−4114	1/1030	103.0	6.5	3.4	–	2.7182	–	O	0.0000	0.17	0.32	0.3852	0.53	1.39
J0828−3417	10/296	14.5	41.4	1.0	11.5	–	Y	–	0.0021	0.35	1.00	0.0000	1.09	2.48
J0831−4406	1/1810	32.1	6.4	0.6	–	–	–	L	0.9425	0.18	0.62	0.5718	0.87	1.96
J0835−3707	6/1023	31.6	13.2	0.7	9.7	–	–	U	0.9934	0.17	0.67	0.9497	0.87	2.05
J0835−4510*	6206/6259	18957.3	22.1	146.1	17.2	0.0649	N	O	0.0000	0.05	0.07	0.0000	0.11	1.05
J0837−4135	726/737	2139.3	149.0	45.1	12.6	0.5839	–	M	0.0063	0.14	0.20	0.0000	0.36	1.25
J0840−5332	2/779	63.1	6.7	1.5	–	–	–	L	0.8239	0.14	0.40	0.1862	0.51	1.53
J0842−4851	2/874	44.1	8.5	1.0	5.6	–	–	L	0.8862	0.15	0.65	0.1996	0.72	1.96
J0846−3533	219/490	138.7	18.9	5.3	5.7	0.6191	–	L	0.9933	0.10	0.20	0.7240	0.29	1.25
J0855−3331	57/443	65.4	16.4	2.2	6.0	–	Y	–	0.0017	0.26	0.42	0.4117	0.94	1.48
J0902−6325	1/842	36.7	6.2	1.1	–	–	–	O	0.0548	0.06	0.55	0.0153	0.28	1.72
J0904−4246	5/564	29.7	9.7	1.0	5.3	–	–	L	0.9844	0.19	0.45	0.6663	0.72	1.63
J0907−5157	1170/2208	456.0	29.0	7.2	10.6	0.8975	–	O	0.0048	0.15	0.12	0.0000	0.38	1.10
J0908−4913	4619/5224	102.8	40.3	7.5	7.2	0.4716	–	O	0.0000	0.09	0.15	0.0008	0.22	1.15
(i)	–	–	–	0.6	7.2	0.4807	N	O	0.0002	0.14	0.87	0.3194	0.80	2.43
(m)	–	–	–	8.7	–	0.4716	N	O	0.0000	0.09	0.17	0.0000	0.25	1.20
J0922−4949	2/591	24.6	7.9	0.8	5.5	–	–	O	0.0251	0.04	0.65	0.0032	0.13	1.91
J0924−5302	1/614	48.0	6.7	1.5	4.4	–	–	L	0.9909	0.09	0.35	0.6844	0.26	1.44
J0924−5814	36/724	69.5	9.2	2.6	5.0	–	–	O	0.6873	0.14	0.35	0.0000	0.41	1.44
J0934−5249	349/385	221.7	51.9	8.5	11.4	0.8599	Y	(U)	1.0000	0.10	0.20	0.9613	0.28	1.25
J0942−5552	445/842	327.2	41.9	9.0	4.8	0.8019	–	M	0.0087	0.22	0.15	0.0000	0.53	1.10
J0942−5657	198/682	121.5	12.7	2.9	4.7	0.6559	–	L	0.9973	0.10	0.27	0.6542	0.33	1.29
J0945−4833	1/1687	32.0	6.6	0.6	–	–	–	U	0.9988	0.17	0.65	0.9885	0.83	2.01
J0955−5304	12/652	40.4	9.0	1.3	5.2	–	–	U	0.9993	0.21	0.37	0.9230	0.79	1.44
J1001−5507	376/386	410.8	45.4	14.5	5.2	0.4926	N	U	0.8644	0.13	0.15	0.9681	0.34	1.15
J1001−5559	1/334	31.2	6.2	1.4	–	–	–	O	0.0523	0.02	0.45	0.0036	0.09	1.58
J1001−5939	18/70	21.9	15.8	1.0	4.1	–	–	O	0.3614	1.07	−0.85	0.2075	0.17	1.05
J1003−4747	1/1823	47.6	6.5	0.9	–	–	–	O	0.1650	0.22	0.35	0.1353	0.86	1.44
J1012−5830	1/262	6.0	6.2	0.3	–	–	Y	–	0.0365	0.04	1.07	0.0010	0.49	2.95
J1012−5857	150/683	108.0	26.1	3.0	6.4	1.0507	–	O	0.6336	0.14	0.30	0.0001	0.40	1.34
J1013−5934	51/1268	78.3	11.9	2.1	5.0	–	–	L	0.9548	0.14	0.30	0.4019	0.43	1.39
J1016−5345	61/729	76.5	13.8	2.0	5.7	–	–	L	0.9809	0.21	0.17	0.6692	0.59	1.20
J1017−5621	157/1105	84.0	17.4	1.9	7.3	–	–	L	0.8495	0.15	0.32	0.0009	0.45	1.39
J1020−5921	4/448	22.6	9.5	0.8	6.8	–	–	L	0.9745	0.25	0.37	0.7425	1.03	1.44
J1032−5206	2/231	24.4	7.3	1.3	5.1	–	–	L	0.9552	0.09	0.45	0.4127	0.25	1.58
J1032−5911	4/1214	50.6	7.5	1.2	–	–	–	O	0.0694	0.23	0.45	0.6103	0.98	1.53
J1036−4926	65/1096	78.5	12.5	1.8	6.3	–	–	L	0.7617	0.09	0.35	0.0531	0.28	1.44
J1038−5831	2/846	30.7	7.2	0.8	4.7	–	–	M	0.2974	0.11	0.45	0.0517	0.41	1.63
J1042−5521	31/479	76.4	10.3	2.7	4.5	–	–	L	0.9559	0.14	0.17	0.3674	0.40	1.20
J1043−6116	68/1930	44.8	13.6	0.7	4.8	–	–	O	0.0076	0.18	0.70	0.0009	0.92	2.05
J1046−5813	3/1525	67.4	7.2	1.4	–	–	–	U	0.9953	0.11	0.42	0.8222	0.40	1.58
J1047−6709	173/2836	76.8	139.7	1.2	19.5	–	–	O	0.0000	0.11	1.60	0.0000	1.09	3.95
J1048−5832	2235/4561	408.5	41.0	4.8	13.1	1.1688	–	M	0.0000	0.33	0.07	0.0000	0.64	0.96
J1049−5833	54/239	40.5	11.0	2.0	5.8	–	Y	–	0.0004	0.35	0.35	0.0000	1.09	1.29
J1055−6905	22/188	33.2	10.2	1.8	4.6	–	Y	–	0.2285	0.31	0.40	0.0061	1.09	1.34
J1056−6258	1225/1326	974.0	39.9	22.3	9.5	0.4494	N	O	0.0000	0.06	0.12	0.0692	0.17	1.15
J1057−5226	237/2847	57.9	34.2	1.7	14.8	–	–	O	0.0217	0.15	0.60	0.3086	0.63	1.86
(i)	–	–	–	1.0	–	–	N	O	0.0284	0.13	0.87	0.0000	0.72	2.48
(m)	–	–	–	1.1	14.8	–	N	O	0.0058	0.30	0.10	0.0001	0.94	1.10
J1059−5742	91/454	75.1	17.1	2.6	8.8	–	Y	(M)	0.8808	0.14	0.22	0.0728	0.38	1.25

Table 1 – *continued*

(1) PSR Jname	(2) Npulses	(3) S/N (int)	(4) S/N (SP)	(5) $\langle s_E \rangle$	(6) Max. R_j	(7) Min. m_j	(8) Null?	(9) Dist. class	(10) P_ℓ	(11) σ_ℓ	(12) μ_ℓ	(13) P_g	(14) σ_g	(15) μ_g
J1104−6103	5/2008	18.1	12.6	0.3	7.1	–	–	O	0.1278	0.26	1.02	0.0000	1.09	2.95
J1106−6438	2/200	18.8	6.7	0.9	–	–	–	U	0.9981	0.10	0.25	0.8714	0.38	1.29
J1107−5907	1/2220	4.5	6.2	0.0	–	–	Y	–	0.0000	1.07	1.97	0.0000	0.24	3.76
J1110−5637	175/1006	153.6	18.4	4.3	6.6	0.9004	–	O	0.7491	0.10	0.17	0.0950	0.28	1.20
J1112−6926	9/679	68.9	9.7	2.2	5.2	–	–	L	0.8444	0.09	0.27	0.3124	0.26	1.34
J1114−6100	94/639	109.2	14.6	3.8	4.8	1.1906	–	L	0.9568	0.22	0.12	0.0096	0.53	1.10
J1117−6154	7/1099	42.1	9.4	1.1	–	–	–	O	0.4040	0.07	0.40	0.1030	0.22	1.53
J1123−4844	100/2276	93.6	10.6	1.8	4.8	–	–	O	0.0089	0.13	0.25	0.0000	0.40	1.34
J1123−6102	5/871	55.0	10.1	1.5	5.5	–	–	U	0.9846	0.15	0.32	0.9179	0.49	1.44
J1126−6054	21/2742	76.5	10.0	1.1	6.0	–	–	G	0.0273	0.19	0.35	0.7906	0.67	1.48
J1129−53	6/525	6.5	31.3	0.2	9.9	–	Y	–	0.3768	0.30	1.42	0.1604	0.05	3.67
J1133−6250	93/551	112.8	20.6	5.2	5.3	1.3483	Y	–	0.1134	0.17	0.25	0.5942	0.49	1.25
J1136−5525	81/1520	122.5	17.3	2.7	6.5	1.7026	–	O	0.0000	0.13	0.30	0.0897	0.41	1.34
J1143−5158	6/829	27.2	10.1	0.7	5.2	–	–	O	0.0436	0.19	0.55	0.0345	0.78	1.91
J1146−6030	30/2045	99.5	18.9	2.0	10.1	–	–	M	0.4683	0.13	0.32	0.0043	0.43	1.39
J1152−6012	4/1489	25.1	8.6	0.5	–	–	–	L	0.9999	0.18	1.22	0.0000	1.09	3.52
J1157−6224	339/1408	203.0	25.5	4.1	7.2	1.1461	Y	–	0.0000	0.17	0.20	0.0416	0.47	1.20
J1202−5820	287/1233	164.1	21.1	3.5	7.9	0.9868	–	L	0.9970	0.14	0.20	0.0024	0.40	1.25
J1215−5328	1/884	23.4	7.0	0.7	4.7	–	–	O	0.4205	0.05	0.65	0.1644	0.26	1.91
J1224−6407	1801/2573	430.1	38.6	7.0	14.5	0.7175	N	O	0.0000	0.09	0.17	0.0000	0.26	1.20
J1225−6035	5/889	24.9	7.5	0.6	–	–	Y	–	0.8720	0.11	0.82	0.5116	0.59	2.39
J1225−6408	2/1327	73.8	7.1	1.8	–	–	–	O	0.1341	0.09	0.15	0.0068	0.24	1.20
J1231−6303	1/407	48.0	6.2	2.2	4.6	–	–	O	0.4088	0.14	0.25	0.0394	0.43	1.29
J1239−6832	11/435	37.9	8.7	1.4	5.8	–	–	L	0.9460	0.19	0.25	0.1745	0.60	1.34
J1243−6423	1268/1448	1786.4	76.1	31.4	5.1	0.5690	Y	(M)	0.0000	0.29	0.25	0.0000	0.64	1.15
J1252−6314	27/684	22.3	11.3	0.7	5.2	–	–	L	0.9838	0.35	0.25	0.2636	1.09	1.44
J1253−5820	141/2190	168.1	10.6	2.7	6.0	1.0648	–	L	0.7623	0.13	0.15	0.1696	0.37	1.20
J1255−6131	1/847	5.8	9.9	0.1	5.8	–	Y	–	0.9963	0.10	1.97	0.0000	1.09	3.95
J1259−6741	85/840	80.1	17.0	2.3	6.0	–	–	L	0.9356	0.21	0.17	0.0118	0.57	1.20
J1306−6617	138/1183	155.6	19.6	3.8	–	1.2613	–	M	0.0407	0.15	0.25	0.0141	0.45	1.25
J1307−6318	11/111	22.8	9.9	2.1	4.6	–	Y	–	0.9127	0.35	0.25	0.8660	1.09	1.01
J1312−5516	3/664	46.4	6.4	1.5	4.5	–	–	O	0.6515	0.09	0.37	0.2849	0.33	1.48
J1314−6101	1/192	17.8	7.5	1.0	–	–	–	O	0.2115	0.41	0.25	0.0701	1.09	1.34
J1320−5359	2/1985	76.6	7.7	1.6	–	–	–	U	0.9936	0.11	0.40	0.8477	0.40	1.53
J1324−6302	1/196	13.4	6.7	0.8	–	–	–	L	0.9973	0.26	0.72	0.3508	1.09	2.05
J1326−5859	972/1101	964.9	36.7	21.6	4.7	0.3409	Y	(L)	0.8518	0.07	0.12	0.0000	0.20	1.10
J1326−6408	90/704	92.7	12.1	2.5	4.8	–	Y	–	0.5453	0.19	0.17	0.4103	0.52	1.20
J1326−6700	682/1022	402.1	31.5	12.4	7.1	0.8457	–	M	0.0000	0.15	0.27	0.0000	0.45	1.29
J1327−6222	980/1062	1412.3	76.2	33.0	5.5	0.4381	N	M	0.0478	0.15	0.15	0.0001	0.37	1.10
J1327−6301	89/2867	127.4	15.0	1.8	–	1.8150	–	O	0.0000	0.15	0.40	0.0557	0.56	1.53
J1327−6400	9/1997	10.7	9.9	0.2	–	–	–	O	0.0906	0.09	1.50	0.0000	1.09	3.95
J1328−4921	2/377	28.4	6.7	1.3	–	–	–	L	0.9948	0.07	0.47	0.6989	0.26	1.63
J1338−6204	13/452	116.3	9.4	5.4	4.5	1.1405	N	L	0.8890	0.07	0.12	0.2629	0.20	1.10
J1340−6456	48/1470	53.9	26.9	1.3	12.6	–	–	O	0.0591	0.11	0.67	0.0000	0.47	2.01
J1341−6023	2/894	42.6	7.6	1.0	–	–	–	L	0.8118	0.11	0.50	0.5079	0.47	1.72
J1345−6115	15/423	35.4	10.3	1.4	4.8	–	–	O	0.2355	0.06	0.32	0.0210	0.16	1.39
J1347−5947	13/898	43.0	13.9	1.1	6.8	–	–	O	0.6197	0.18	0.47	0.0016	0.68	1.67
J1355−5153	36/870	86.5	12.5	2.0	6.8	–	–	O	0.5448	0.09	0.27	0.0695	0.29	1.34
J1357−62	690/1236	396.5	12.0	11.0	5.1	0.5327	N	O	0.2966	0.06	0.15	0.0000	0.16	1.15
J1359−6038	2863/4407	541.4	18.3	4.5	–	0.3342	–	O	0.0023	0.07	0.15	0.0003	0.20	1.15
J1401−6357	610/656	603.2	109.5	15.2	11.4	0.7267	–	M	0.9663	0.18	0.07	0.0000	0.38	1.01
J1406−5806	111/1927	21.1	27.2	0.4	8.6	–	Y	–	0.0000	0.25	1.45	0.0000	1.09	3.95
J141−7404	21/2000	79.7	12.0	1.0	6.3	–	–	O	0.0414	0.11	0.57	0.0007	0.45	1.86
J1413−6307	32/1408	57.5	22.6	1.1	9.9	–	–	U	0.9496	0.18	0.57	0.9941	0.80	1.82
J1414−6802	9/112	37.0	10.1	2.7	4.8	–	–	O	0.5113	0.17	0.25	0.0663	0.45	1.39
J1416−6037	6/1903	24.6	9.8	0.5	–	–	–	U	0.9577	0.19	0.80	0.8583	1.09	2.29
J1423−6953	108/1676	35.6	43.6	0.5	12.4	–	Y	–	0.0003	0.17	0.97	0.0000	0.99	2.91
J1428−5530	613/984	269.2	38.8	7.2	11.6	0.7993	Y	(L)	0.9972	0.11	0.22	0.0000	0.32	1.25
J1430−6623	680/708	1315.8	78.4	38.3	11.2	0.4381	N	L	0.8144	0.15	0.15	0.0000	0.36	1.10
J1439−5501	1/10000	9.5	6.1	0.1	–	–	–	O	0.0000	0.65	1.97	0.0000	0.10	2.81
J1440−6344	2/1228	67.9	6.5	1.6	–	–	–	O	0.1214	0.13	0.30	0.0352	0.40	1.39

Table 1 – *continued*

(1) PSR Jname	(2) Npulses	(3) S/N (int)	(4) S/N (SP)	(5) $\langle s_E \rangle$	(6) Max. R_j	(7) Min. m_j	(8) Null?	(9) Dist. class	(10) P_ℓ	(11) σ_ℓ	(12) μ_ℓ	(13) P_g	(14) σ_g	(15) μ_g
J1444−5941	2/204	16.1	7.1	0.7	–	–	–	O	0.7104	0.05	1.17	0.0968	0.22	3.14
J1452−6036	86/3577	64.0	19.3	0.6	7.6	–	–	O	0.0000	0.26	0.70	0.0000	1.09	2.15
J1453−6413	1828/3107	889.5	23.5	9.5	6.0	0.5077	Y	(L)	0.7562	0.10	0.22	0.0000	0.28	1.25
J1456−6843	1218/2124	1077.9	41.8	21.5	15.8	0.8839	–	O	0.0000	0.17	0.27	0.0000	0.43	1.25
J1457−5122	54/315	43.4	37.4	2.0	9.3	–	Y	–	0.2639	0.38	0.22	0.0066	1.09	0.86
J1502−5653	96/1050	45.2	16.6	1.0	5.6	–	Y	–	0.0000	0.11	0.27	0.0000	0.26	1.48
J1507−4352	1584/1952	380.6	19.0	6.2	6.2	0.4956	–	G	0.0087	0.09	0.22	0.8712	0.24	1.25
J1507−6640	117/1576	107.8	12.0	1.6	6.4	1.2561	–	L	0.7522	0.17	0.50	0.4182	0.64	1.67
J1512−5759	11/4367	189.8	7.9	2.0	–	0.9679	–	O	0.0053	0.14	0.20	0.0435	0.40	1.25
J1514−4834	123/1224	99.6	10.9	2.4	–	–	Y	–	0.3051	0.14	0.17	0.0051	0.40	1.20
J1514−59	2/533	5.7	6.6	0.1	–	–	Y	–	0.1941	0.11	1.97	0.0000	1.09	3.95
J1522−5829	474/1429	244.5	12.9	5.9	5.9	0.7823	–	O	0.0470	0.11	0.12	0.0158	0.30	1.15
J1527−3931	40/227	64.9	12.8	3.3	5.9	–	Y	–	0.9552	0.13	0.17	0.1991	0.36	1.25
J1527−5552	6/535	48.7	7.5	1.6	4.5	–	–	O	0.5225	0.02	0.20	0.0595	0.10	1.25
J1528−4109	2/1063	28.3	7.5	0.7	–	–	–	U	0.9792	0.17	0.65	0.8310	0.84	2.01
J1530−5327	6/1992	40.7	7.8	0.8	4.8	–	–	O	0.0364	0.17	0.60	0.0495	0.74	1.91
J1534−5334	301/410	194.1	24.4	6.6	4.8	0.4798	N	L	0.9280	0.11	0.05	0.0522	0.28	1.05
J1534−5405	1/1940	63.0	6.4	1.3	–	–	–	O	0.0049	0.11	0.37	0.0000	0.37	1.48
J1535−4114	16/1290	75.1	12.7	1.8	8.3	–	–	O	0.0772	0.14	0.25	0.0583	0.44	1.34
J1535−5848	1/1824	24.3	7.5	0.5	5.2	–	–	U	0.9606	0.26	0.45	0.7970	1.09	1.67
J1536−5433	6/638	43.2	8.3	1.6	5.2	–	–	O	0.0000	0.07	0.37	0.0000	0.28	1.44
J1539−5626	7/2299	103.9	6.8	2.0	–	1.8576	–	O	0.1407	0.13	0.35	0.0096	0.40	1.44
J1539−6322	9/345	58.0	8.8	2.7	–	–	–	M	0.8521	0.11	0.40	0.2512	0.37	1.48
J1542−5303	6/468	10.5	11.6	0.4	–	–	–	L	0.9764	0.19	0.85	0.4618	1.09	2.48
J1544−5308	2/3162	88.2	9.0	1.2	–	–	–	O	0.5381	0.13	0.42	0.1461	0.47	1.58
J1548−4927	86/934	62.0	19.7	1.5	7.9	–	–	L	0.9758	0.23	0.45	0.0014	0.91	1.53
J1553−5456	8/522	33.4	10.6	1.2	–	–	–	O	0.3615	0.06	0.32	0.0617	0.11	1.44
J1556−5358	1/561	21.4	6.8	0.8	–	–	–	O	0.0368	0.05	0.60	0.0054	0.14	1.86
J1557−4258	76/1701	104.1	12.7	1.8	4.8	1.3912	–	O	0.5319	0.14	0.32	0.3982	0.47	1.39
J1559−4438	561/2169	514.1	17.4	9.3	7.3	0.4438	N	O	0.0000	0.05	0.17	0.0000	0.14	1.20
J1559−5545	10/305	33.8	10.6	1.3	4.8	–	Y	–	0.9392	0.27	0.30	0.5304	0.94	1.34
J1600−5044	2362/2899	721.5	28.3	10.5	–	0.4560	–	O	0.0000	0.11	0.15	0.6171	0.30	1.15
J1602−5100	513/652	252.3	41.2	7.5	9.1	0.7918	–	M	0.0368	0.13	0.17	0.0000	0.36	1.20
J1603−5657	13/1126	98.9	7.9	1.7	–	–	–	L	0.9654	0.09	0.27	0.5089	0.29	1.34
J1604−4909	328/1725	165.8	13.7	3.0	5.6	0.9248	–	O	0.4132	0.14	0.32	0.0000	0.45	1.39
J1605−5257	224/847	315.6	19.1	11.2	10.8	0.8175	–	L	0.9943	0.11	0.15	0.0571	0.30	1.15
J1611−5847	1/1578	17.4	6.2	0.3	–	–	–	L	0.9129	0.07	1.72	0.0000	0.02	3.86
J1615−5444	4/1549	33.4	6.9	0.8	–	–	–	L	0.7997	0.26	0.35	0.0040	0.95	1.48
J1615−5537	1/686	15.8	7.2	0.4	6.5	–	–	O	0.5578	0.15	0.52	0.1792	0.68	1.77
J1621−5039	1/514	13.5	11.0	0.5	6.0	–	–	L	0.8536	0.31	0.45	0.2189	1.09	1.86
J1622−4950	75/130	263.3	22.5	22.9	6.4	0.5474	–	O	0.0156	0.13	0.12	0.0035	0.32	1.15
J1624−4613	10/636	13.2	9.8	0.5	4.8	–	Y	–	0.8338	0.43	0.45	0.1425	1.09	1.44
J1625−4048	6/230	27.7	7.6	1.6	–	–	–	U	0.9853	0.18	0.45	0.7576	0.72	1.67
J1626−4537	2/1515	43.4	7.6	1.0	–	–	–	L	0.8209	0.22	0.35	0.2921	0.78	1.48
J1632−4621	1/325	26.3	6.1	0.9	–	–	–	L	0.9188	0.18	0.47	0.5621	0.75	1.67
J1633−4453	47/1285	57.2	9.1	1.4	–	–	Y	–	0.0163	0.35	0.37	0.0000	1.09	1.10
J1633−5015	867/1590	340.1	22.1	7.3	–	0.5949	–	O	0.0000	0.15	0.15	0.1412	0.38	1.15
J1644−4559	1225/1237	8209.0	43.5	186.1	7.5	0.1741	N	O	0.0000	0.07	0.07	0.0002	0.20	1.05
J1646−6831	195/312	248.1	64.9	12.5	9.9	1.0749	Y	–	0.0000	0.63	0.40	0.0000	1.09	0.20
J1647−36	22/2672	9.5	15.1	0.2	6.5	–	Y	(L)	0.8319	0.22	1.47	0.0000	0.13	3.48
J1648−3256	52/764	97.0	9.8	2.4	4.7	–	–	L	0.9798	0.07	0.15	0.4164	0.18	1.20
J1649−4349	4/639	19.4	6.9	0.7	4.7	–	Y	–	0.0034	0.41	0.55	0.0000	1.09	1.67
J1651−4246	147/664	385.8	12.8	14.8	7.1	0.6205	N	M	0.0002	0.10	0.12	0.0034	0.26	1.15
J1651−5222	290/878	157.5	15.0	4.1	4.9	0.8903	–	G	0.0702	0.15	0.17	0.7991	0.41	1.20
J1651−5255	4/633	58.6	6.2	1.9	4.5	–	–	L	0.9433	0.11	0.22	0.5034	0.36	1.29
J1653−3838	188/1848	110.0	30.6	2.3	7.6	1.6457	Y	–	0.0012	0.15	0.32	0.0000	0.47	1.39
J1653−4249	2/918	48.5	7.6	1.3	–	–	–	O	0.0121	0.07	0.32	0.0015	0.26	1.39
J1653−4854	1/182	11.8	7.3	0.6	–	–	–	L	0.8089	0.30	0.92	0.7055	1.09	2.72
J1654−23	11/1036	10.9	13.5	0.3	9.1	–	–	L	0.9931	0.30	1.02	0.0000	1.09	3.00
J1654−4140	3/427	24.3	7.0	1.0	4.6	–	–	M	0.0125	0.14	0.57	0.0023	0.64	1.82
J1700−3312	62/357	65.8	16.1	2.7	8.0	–	–	L	0.9846	0.15	0.25	0.5991	0.44	1.29

Table 1 – *continued*

(1) PSR Jname	(2) Npulses	(3) S/N (int)	(4) S/N (SP)	(5) $\langle s_E \rangle$	(6) Max. R_j	(7) Min. m_j	(8) Null?	(9) Dist. class	(10) P_ℓ	(11) σ_ℓ	(12) μ_ℓ	(13) P_g	(14) σ_g	(15) μ_g
J1700−3611	2/371	28.6	7.9	1.1	4.5	–	–	O	0.6352	0.13	0.35	0.1433	0.38	1.44
J1701−3130	7/1929	55.5	8.2	1.1	–	–	–	U	0.9928	0.15	0.40	0.9647	0.56	1.58
J1701−3726	139/224	119.5	18.9	6.6	7.3	0.8977	Y	–	0.0000	1.07	1.27	0.2732	0.36	1.86
J1701−4533	1/1720	115.1	6.9	2.8	4.9	1.8759	–	O	0.0917	0.13	0.25	0.5211	0.36	1.29
J1703−3241	405/405	314.6	43.2	13.6	7.2	0.5948	Y	(M)	0.0011	0.07	0.15	0.0000	0.20	1.15
J1703−4442	2/318	10.8	9.2	0.5	5.7	–	–	O	0.6385	0.05	0.65	0.1818	0.11	2.05
J1705−1906	872/1867	242.5	18.8	13.6	9.6	0.4264	N	O	0.0000	0.17	0.15	0.0000	0.40	1.10
(i)	–	–	–	1.8	8.3	0.7883	N	L	0.9997	0.13	0.65	0.0011	0.59	1.96
(m)	–	–	–	14.2	9.6	0.4264	N	O	0.0000	0.18	−0.00	0.0000	0.37	0.96
J1705−3423	187/2238	188.1	10.4	3.8	5.3	1.3555	–	O	0.0029	0.15	0.12	0.1837	0.40	1.15
J1705−3950	7/1746	35.6	9.8	0.7	4.8	–	–	L	0.8104	0.26	0.50	0.0063	1.09	1.72
J1706−6118	119/1534	52.1	34.5	0.8	8.7	–	–	O	0.6280	0.17	0.72	0.0000	0.75	2.24
J1707−4053	16/960	124.9	9.2	3.5	–	1.3939	–	O	0.6191	0.10	0.25	0.3935	0.29	1.29
J1707−44	3/98	13.5	8.2	1.1	5.3	–	–	L	0.9345	0.09	0.70	0.7019	0.48	2.05
J1707−4729	68/2084	60.8	14.2	1.3	–	–	Y	–	0.0000	0.31	0.37	0.1334	1.09	1.34
J1708−3426	19/802	62.2	10.9	1.9	5.6	–	–	O	0.3210	0.15	0.22	0.0445	0.45	1.29
J1709−1640	627/857	386.2	37.2	10.1	12.9	0.7796	Y	–	0.0000	0.21	0.25	0.0006	0.60	1.20
J1709−4429	31/5438	198.3	7.5	2.3	5.9	1.3016	–	O	0.0001	0.13	0.22	0.0001	0.38	1.29
J1711−5350	7/614	53.2	7.9	1.6	–	–	–	L	0.9692	0.15	0.35	0.6167	0.53	1.44
J1715−4034	14/270	49.5	11.3	2.7	–	–	–	O	0.0401	0.18	0.25	0.0004	0.53	1.34
J1717−3425	2/848	94.3	7.0	2.8	–	–	–	O	0.2274	0.02	0.20	0.0019	0.09	1.20
J1717−4043	7/1416	17.4	8.2	0.5	–	–	–	L	0.8154	0.23	0.87	0.0000	1.09	2.58
J1718−3825	1/7607	29.5	7.7	0.3	–	–	–	O	0.0000	0.30	1.27	0.0000	1.09	3.76
J1720−2933	1/885	31.5	6.4	0.9	5.0	–	–	L	0.8275	0.09	0.42	0.4992	0.26	1.53
J1721−3532	15/1987	220.1	7.9	4.6	4.9	1.4397	–	O	0.0000	0.15	0.22	0.0001	0.44	1.25
J1722−3207	652/1170	265.2	50.0	6.8	14.9	0.7151	N	O	0.1234	0.09	0.20	0.0000	0.25	1.20
J1722−3632	1/1413	37.9	6.5	1.0	–	–	–	O	0.4579	0.21	0.47	0.3012	0.84	1.67
J1722−3712	241/2382	214.7	10.3	3.3	–	0.8111	–	O	0.0361	0.05	0.65	0.1161	0.22	1.96
J1723−3659	1/2740	38.5	14.5	0.7	–	–	–	G	0.0745	0.25	0.42	0.7637	1.01	1.63
J1725−4043	8/368	18.4	15.5	0.8	8.1	–	Y	–	0.9392	0.34	0.60	0.0040	1.09	1.77
J1727−2739	127/434	74.6	28.4	3.8	7.3	–	Y	–	0.0000	0.57	0.52	0.0026	1.09	0.91
J1730−3350	22/4057	83.4	12.6	1.0	4.8	–	–	O	0.0000	0.26	0.57	0.0103	1.09	1.72
J1731−4744	593/674	1167.8	106.8	33.1	13.9	0.5113	N	L	0.9826	0.14	0.15	0.0055	0.36	1.15
J1732−4156	1/1736	8.7	8.4	0.2	6.0	–	–	O	0.0762	0.46	0.90	0.0000	1.09	3.95
J1733−2228	19/645	136.4	7.8	5.3	4.7	1.0549	–	L	0.8932	0.09	0.15	0.1185	0.24	1.20
J1733−3716	146/1663	53.8	32.9	1.4	9.9	–	–	O	0.0002	0.23	0.32	0.0000	0.74	1.39
J1735−0724	13/1318	96.8	7.0	2.3	–	–	–	U	0.9983	0.09	0.45	0.9913	0.32	1.58
J1736−2457	25/211	40.3	11.4	2.2	4.6	–	Y	–	0.9564	0.21	0.22	0.2750	0.56	1.25
J1737−3555	3/1417	30.8	7.0	0.7	–	–	–	O	0.6267	0.22	0.52	0.0172	0.92	1.77
J1738−2330	7/277	13.1	8.1	0.7	4.8	–	Y	–	0.9480	0.33	0.40	0.5859	1.06	1.82
J1738−3211	162/732	105.7	27.9	2.9	14.6	1.3554	Y	–	0.0496	0.17	0.32	0.1170	0.52	1.39
J1739−2903	104/1739	82.2	20.8	2.1	11.6	–	–	O	0.0024	0.13	0.25	0.0000	0.38	1.29
(i)	–	–	–	0.9	–	–	N	L	0.9197	0.14	0.55	0.5745	0.55	1.82
(m)	–	–	–	1.9	11.6	–	N	O	0.3612	0.17	0.45	0.0000	0.57	1.58
J1739−3023	1/4870	13.8	6.1	0.1	–	–	–	O	0.0191	0.25	1.35	0.0000	0.13	3.95
J1740−3015	480/919	179.6	19.8	3.5	6.8	0.6859	–	O	0.0574	0.10	0.22	0.0002	0.28	1.29
J1741−0840	154/272	121.7	27.1	6.3	6.6	1.0280	Y	–	0.0000	0.81	0.82	0.0000	1.09	0.20
J1741−2019	29/135	31.6	19.8	2.0	6.3	–	–	O	0.7164	0.21	0.20	0.4152	0.59	1.25
J1741−3016	9/297	41.1	9.3	2.1	4.6	–	Y	–	0.9920	0.14	0.32	0.5881	0.49	1.44
J1741−3927	375/1015	200.4	17.5	5.3	4.7	0.6947	N	M	0.1270	0.11	0.15	0.0000	0.30	1.15
J1742−4616	10/1357	56.2	7.5	1.5	5.3	–	Y	–	0.0000	0.31	0.35	0.0790	1.09	1.25
J1743−3150	86/233	85.5	20.9	4.1	6.3	–	–	L	0.9926	0.19	0.10	0.5792	0.45	1.10
J1744−1134	16/138924	22.4	11.0	0.0	–	–	–	O	0.0000	0.38	1.97	0.0000	0.05	2.34
J1744−1610	3/320	18.5	8.1	0.8	4.8	–	–	L	0.9892	0.22	0.45	0.6995	0.91	1.63
J1744−3130	4/528	18.2	8.0	0.6	4.8	–	–	O	0.0181	0.09	0.32	0.0005	0.22	1.48
J1745−3040	738/1529	408.3	79.5	7.7	11.0	1.3502	Y	–	0.0000	0.34	−0.13	0.0000	0.41	0.72
J1749−5605	22/418	47.7	16.1	1.6	6.4	–	–	O	0.7369	0.17	0.20	0.1151	0.49	1.29
J1750−3157	42/610	41.1	13.3	1.5	5.9	–	Y	–	0.0058	0.27	0.50	0.0935	1.09	1.48
J1751−3323	2/1014	47.7	8.4	1.3	–	–	–	O	0.7010	0.15	0.30	0.3216	0.51	1.39
J1751−4657	179/739	133.6	31.9	3.6	13.3	0.9885	–	L	0.9992	0.11	0.45	0.2437	0.43	1.58
J1752−2806	938/995	1304.1	66.7	26.6	8.3	0.4962	N	O	0.0531	0.21	0.12	0.0000	0.48	1.10

Table 1 – *continued*

(1) PSR Jname	(2) Npulses	(3) S/N (int)	(4) S/N (SP)	(5) $\langle s_E \rangle$	(6) Max. R_j	(7) Min. m_j	(8) Null?	(9) Dist. class	(10) P_ℓ	(11) σ_ℓ	(12) μ_ℓ	(13) P_g	(14) σ_g	(15) μ_g
J1753−38	14/848	20.1	16.0	0.4	8.8	–	–	O	0.0820	0.38	0.22	0.0000	1.09	1.72
J1754−3510	31/1421	41.2	11.0	0.8	6.1	–	–	O	0.3901	0.18	0.57	0.0259	0.80	1.86
J1755−2521	1/465	16.7	9.2	0.6	4.4	–	–	L	0.8487	0.10	0.77	0.3250	0.53	2.29
J1756−2225	9/1387	11.4	10.9	0.3	–	–	–	L	0.9745	0.19	1.27	0.0001	1.09	3.81
J1756−2435	1/827	70.6	6.5	2.2	–	–	–	O	0.0273	0.14	0.17	0.0176	0.38	1.20
J1757−2223	40/3042	17.5	19.7	0.2	8.6	–	Y	–	0.0284	0.27	1.00	0.0000	1.09	3.95
J1757−2421	168/2380	197.4	17.4	3.6	9.1	1.3102	–	O	0.7076	0.10	0.27	0.0242	0.32	1.29
J1758−2540	12/266	32.6	8.7	1.9	–	–	Y	–	0.0028	0.66	0.82	0.0017	1.09	1.10
J1758−2846	1/725	13.8	6.1	0.4	–	–	–	O	0.1359	0.05	0.90	0.0358	0.18	2.53
J1759−1956	19/194	43.1	9.7	2.0	5.9	–	–	O	0.6426	0.21	0.37	0.0449	0.68	1.48
J1759−2205	181/1222	133.1	15.1	2.1	5.0	0.7153	–	O	0.0001	0.09	0.27	0.0000	0.25	1.29
J1759−3107	13/511	48.9	8.9	1.6	–	–	–	U	0.9915	0.14	0.32	0.8948	0.47	1.44
J1801−2920	42/514	48.5	18.3	1.9	7.6	–	–	L	0.9067	0.18	0.45	0.0076	0.67	1.53
J1803−1857	7/191	29.2	12.3	1.3	4.3	–	–	O	0.7172	0.11	0.37	0.1624	0.41	1.48
J1803−2137	67/4166	158.6	11.7	1.9	5.3	1.7331	–	O	0.0000	0.21	0.40	0.0000	0.69	1.44
J1805−1504	1/357	81.2	6.4	4.3	–	–	–	U	0.8400	0.15	0.30	0.9497	0.47	1.34
J1806−1154	1/1071	75.8	6.1	2.2	–	–	–	L	0.9721	0.13	0.22	0.2183	0.36	1.29
J1807−0847	824/3403	390.2	10.9	5.4	5.9	0.4645	–	G	0.0105	0.07	0.20	0.7922	0.20	1.25
J1807−2715	11/676	56.2	11.4	1.7	4.7	–	–	U	0.9929	0.11	0.30	0.8543	0.37	1.39
J1808−0813	2/629	53.0	8.4	1.8	–	–	Y	–	0.0425	0.18	0.30	0.1071	0.60	1.39
J1808−2057	41/603	108.3	11.9	3.2	4.5	1.1464	–	L	0.9894	0.15	0.20	0.2860	0.43	1.25
J1808−3249	3/1544	34.8	6.7	0.8	5.1	–	–	O	0.0001	0.11	0.42	0.0000	0.45	1.58
J1809−2109	35/795	41.0	12.1	1.0	6.6	–	Y	–	0.0181	0.38	0.52	0.0000	1.09	1.48
J1814−0618	1/109	17.6	6.9	1.4	–	–	–	U	0.8606	0.39	0.27	0.9719	1.09	1.10
J1814−1649	1/593	41.7	6.9	1.5	–	–	–	L	0.9840	0.14	0.30	0.5557	0.45	1.39
J1815−1910	1/449	9.2	6.3	0.3	–	–	–	O	0.4623	0.38	0.60	0.0241	1.09	2.24
J1816−1729	3/713	59.4	7.3	1.7	–	–	–	L	0.8081	0.09	0.35	0.1825	0.29	1.44
J1817−3618	279/1453	114.4	29.1	2.3	13.1	1.5808	Y	–	0.0000	0.33	0.22	0.0031	0.92	1.10
J1817−3837	17/1465	85.4	8.3	1.6	4.7	–	–	L	0.9383	0.11	0.40	0.4887	0.37	1.53
J1819−1458	7/132	9.7	16.8	0.5	8.1	–	Y	(L)	0.8941	0.06	0.40	0.3709	0.18	1.53
J1820−0427	913/926	595.9	43.1	14.7	7.0	0.3359	N	L	0.8796	0.09	0.12	0.0151	0.22	1.15
J1820−0509	22/1661	17.8	9.8	0.4	4.9	–	Y	–	0.0477	0.26	1.15	0.0000	1.09	3.33
J1820−1346	29/592	76.5	10.1	2.8	–	–	–	L	0.9107	0.17	0.25	0.1762	0.48	1.29
J1821−1432	1/273	12.9	7.9	0.7	–	–	–	O	0.0125	0.06	0.47	0.0001	0.07	1.67
J1822−2256	175/279	103.3	17.1	5.1	6.5	1.0380	Y	(U)	1.0000	0.10	0.20	0.7840	0.29	1.20
J1823−1126	9/292	20.5	20.6	0.9	7.0	–	Y	(L)	0.9112	0.30	0.12	0.0420	0.40	1.44
J1824−1945	2009/2962	454.2	24.9	5.4	6.2	0.4280	N	O	0.1838	0.09	0.20	0.0000	0.24	1.20
J1824−2233	2/456	21.2	8.2	0.7	–	–	–	O	0.6926	0.49	0.17	0.0162	1.09	1.20
J1824−2328	1/329	25.1	6.8	1.1	–	–	–	L	0.8165	0.22	0.40	0.3816	0.80	1.53
J1825−0935	566/731	358.9	69.5	8.1	14.5	0.7238	–	O	0.4060	0.18	0.20	0.0000	0.47	1.20
(i)	–	–	–	1.0	–	1.9292	N	L	0.9755	0.18	0.52	0.1689	0.68	1.77
(m)	–	–	–	8.3	14.5	0.7238	N	O	0.0166	0.15	0.17	0.0000	0.37	1.15
J1825−1446	236/2016	110.0	50.4	2.2	6.5	2.3894	Y	–	0.0000	0.17	0.27	0.0000	0.41	1.29
J1826−1131	1/267	60.3	7.2	3.3	–	–	–	L	0.9887	0.02	0.30	0.4725	0.07	1.34
J1827−0750	45/2070	48.7	17.9	1.0	5.5	–	Y	–	0.0000	0.17	1.20	0.0000	1.09	3.14
J1829−0734	5/1750	19.6	8.0	0.4	5.1	–	–	O	0.0046	0.25	0.90	0.0000	1.09	2.72
J1829−1751	615/1820	301.7	17.2	6.3	9.0	0.7746	–	L	0.9018	0.09	0.20	0.0016	0.25	1.25
J1830−1059	10/1370	48.3	9.3	0.9	–	–	–	O	0.7474	0.18	0.35	0.5392	0.67	1.48
J1830−1135	16/78	31.0	12.4	2.6	4.6	–	Y	–	0.2407	0.25	0.27	0.2606	0.72	1.24
J1831−1223	15/193	29.2	10.1	1.8	5.0	–	Y	–	0.9205	0.22	0.42	0.2856	0.90	1.48
J1831−1329	3/253	29.2	6.7	1.5	–	–	–	U	0.9920	0.18	0.37	0.7959	0.60	1.48
J1832−0827	111/875	113.6	15.0	2.7	6.3	0.8993	–	L	0.8204	0.13	0.15	0.0827	0.34	1.20
J1833−0338	296/818	153.1	13.9	3.4	9.0	0.6031	–	O	0.2235	0.10	0.15	0.0003	0.26	1.15
J1833−0827	288/6566	110.6	19.4	0.8	–	1.8933	–	O	0.0000	0.27	0.75	0.0000	1.09	2.05
J1833−1055	2/869	15.3	6.6	0.5	–	–	–	O	0.1725	0.35	0.75	0.0000	1.09	2.24
J1834−0426	12/1951	277.3	9.1	6.3	6.3	1.5350	–	O	0.0000	0.09	0.20	0.1849	0.25	1.20
J1835−1020	1/609	40.9	6.7	1.4	–	–	–	U	1.0000	0.13	0.32	0.9650	0.41	1.39
J1835−1106	8/3393	83.3	8.4	0.9	5.1	–	–	L	0.9600	0.11	0.85	0.3537	0.65	2.39
J1836−0436	3/1582	75.1	7.2	1.6	–	–	–	O	0.0684	0.09	0.37	0.0070	0.29	1.48
J1836−1008	255/995	172.2	10.9	4.0	–	0.5883	–	O	0.5187	0.05	0.17	0.0001	0.16	1.20

Table 1 – *continued*

(1) PSR Jname	(2) Npulses	(3) S/N (int)	(4) S/N (SP)	(5) $\langle s_E \rangle$	(6) Max. R_j	(7) Min. m_j	(8) Null?	(9) Dist. class	(10) P_ℓ	(11) σ_ℓ	(12) μ_ℓ	(13) P_g	(14) σ_g	(15) μ_g
J1837−0653	79/290	72.1	24.4	3.5	6.1	–	Y	–	0.0000	0.81	1.30	0.0000	1.09	0.91
J1837−1243	2/285	6.4	8.6	0.2	–	–	Y	–	0.9562	0.33	1.20	0.0432	1.09	3.71
J1839−1238	1/291	25.6	8.1	1.2	5.2	–	–	O	0.1427	0.04	0.40	0.0089	0.13	1.48
J1840−0809	64/568	75.3	12.3	2.5	4.9	–	–	L	0.8623	0.11	0.47	0.5718	0.44	1.63
J1840−0815	55/477	82.2	18.9	2.7	6.7	–	–	L	0.8874	0.13	0.25	0.2749	0.37	1.29
J1840−0840	42/101	72.3	33.2	6.6	6.3	–	Y	–	0.4169	0.49	0.50	0.4267	1.09	0.91
J1840−1417	9/85	28.8	68.9	1.3	7.3	–	Y	–	0.9129	0.05	0.47	0.4385	0.29	1.63
J1841−0157	9/846	47.4	8.2	1.5	5.1	–	–	O	0.5375	0.17	0.35	0.0186	0.53	1.44
J1841−0310	4/334	5.7	9.7	0.3	5.5	–	Y	–	0.9858	0.10	1.25	0.5221	0.53	3.95
J1841−0425	32/3016	128.2	8.9	1.9	–	1.7033	–	O	0.5864	0.10	0.32	0.0001	0.33	1.39
J1842−0359	92/305	110.5	20.4	7.0	6.2	1.1869	–	L	0.9958	0.17	0.20	0.1326	0.44	1.20
J1843−0459	1/734	45.8	6.3	1.6	4.8	–	–	G	0.0409	0.26	0.30	0.8523	0.95	1.29
J1844−0433	53/570	76.6	15.1	2.3	5.6	–	–	O	0.1971	0.15	0.30	0.2807	0.49	1.34
J1845−0434	15/1149	113.5	7.6	2.9	–	1.2484	–	L	0.8873	0.13	0.12	0.1470	0.32	1.15
J1846−07492	1/655	28.2	6.1	0.9	–	–	–	L	0.9840	0.11	0.57	0.5607	0.44	1.82
J1847−0402	59/927	124.3	10.6	3.4	5.1	1.1194	–	O	0.0243	0.09	0.15	0.0002	0.25	1.20
J1847−0605	4/686	13.7	7.3	0.5	5.0	–	–	L	0.9282	0.13	0.72	0.2881	0.59	2.15
J1848−1150	3/417	15.7	8.5	0.6	–	–	–	O	0.3449	0.35	0.40	0.0009	1.09	1.63
J1848−1952	58/122	137.2	91.5	8.0	7.4	1.0877	Y	–	0.0084	0.42	−0.13	0.0175	0.87	0.53
J1852−0635	150/1067	87.7	21.8	2.7	9.1	–	Y	–	0.4344	0.23	0.10	0.0000	0.51	1.10
J1854−1421	149/476	116.8	22.9	4.2	8.7	0.8327	–	O	0.1650	0.15	0.12	0.0351	0.40	1.15
J1857−1027	73/145	92.5	41.0	6.4	7.3	–	Y	–	0.1064	0.34	0.15	0.1667	0.78	1.05
J1900−2600	548/919	385.8	21.9	12.6	8.4	0.7765	–	M	0.0003	0.09	0.27	0.0000	0.29	1.29
J1901−0906	219/313	156.5	58.0	6.8	7.1	0.8386	–	U	1.0000	0.11	0.22	0.9777	0.30	1.25
J1901−1740	5/285	17.3	7.7	0.8	–	–	–	L	0.9654	0.39	0.15	0.5161	1.09	1.15
J1903−0632	8/1304	47.1	9.0	1.0	–	–	–	L	0.7572	0.15	0.47	0.2843	0.61	1.67

*Many single pulses from the Vela pulsar (PSR J0835−4510) saturated the observing instrumentation. This disrupted the observed integrated and single-pulse S/N, and the modulation parameters at phases near the pulse peak. The modulation parameters are not reported here but Vela's modulation profile can be viewed in the online figure (see Supporting Information, Appendix A).

(iv) *Multipeaked (M; 7 per cent)*. As described above, two or more peaks were discernible at energy levels above the noise.

(v) *Other (O; 48 per cent)*. Pulsars with $P_\ell, P_g < 0.75$.

In cases where we had multiple observations on the same pulsar, we only use the observation in which the pulsar's integrated intensity was brightest. It is pertinent to note, however, that in duplicate observations, the modulation statistics were reproducible. In only a few cases the energy distribution had a different classification in the fainter observation, typically transforming an L-class pulsar to an O or U, and likely caused by the stronger influence of noise on the lower S/N observation.

4.2 The distribution statistics of pulse energy

More than one-third of our classifiable sample was found to be above our threshold for agreement with a log-normal distribution. This is accented by Fig. 2, in which we show a comparison of the best-fitting probability for all pulsars. The general tendency of the energies away from a symmetric, Gaussian distribution here is pronounced. The origin of the tail of objects across all probabilities for both the log-normal and Gaussian trials is thought to be a low-S/N effect, and is discussed below. A primary target of this analysis was to determine whether pulsar energy is well fitted to a Gaussian or log-normal distribution, and if so, what distribution parameters are typical. We will focus momentarily on determining the parameters of the log-normal pulsars in our sample. We include unimodal objects in this discussion on the basis of their agreement with a log-normal distribution. The distribution of both σ_ℓ and

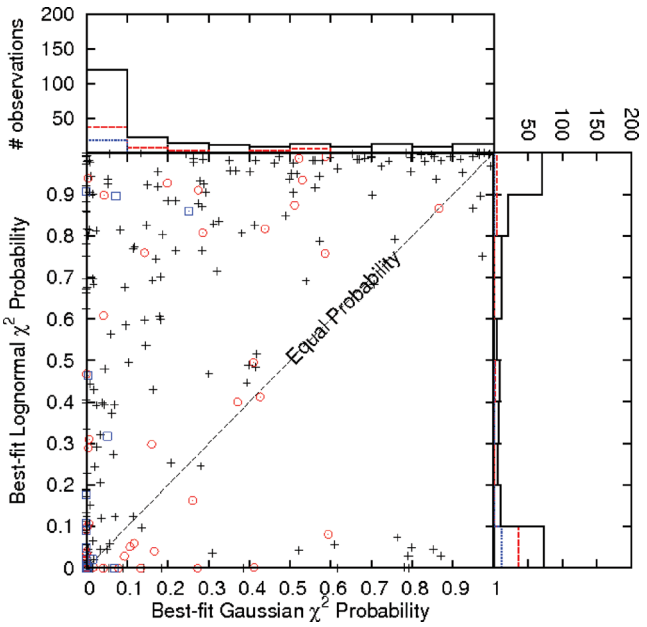

Figure 2. A comparison of our best-fitting distribution probabilities. Log-normal distributions are clearly favoured. All objects classified as G, L, U or O (Section 4.1) are shown as black crosses (solid line), while unclassifiable nulling pulsars are shown as red circles (dashed line) and multipeaked distributions are shown as blue squares (dotted line). The upper and right-hand panels show the integrated distribution of Gaussian and log-normal probabilities, respectively.

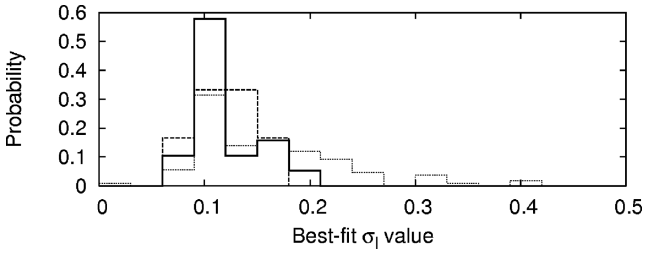

Figure 3. The normalized best-fitting σ_ℓ distribution for strong-signal (thick dark line), non-nulling (dashed line) and all sources under the log-normal classification.

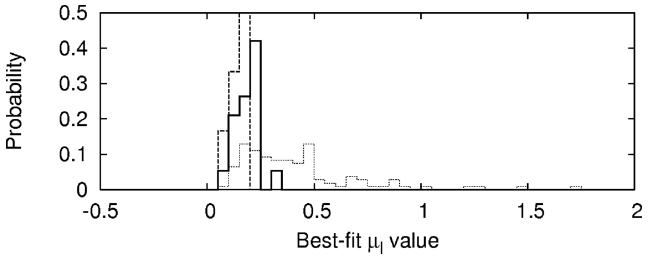

Figure 4. As in Fig. 3, but reporting the best-fitting μ_ℓ.

μ_ℓ is qualitatively similar for the log-normal and unimodal sources [and a Kolmogorov–Smirnov (KS) test between the distributions does not support the null hypothesis].

Care must be taken when considering the σ_ℓ and μ_ℓ results for our log-normal targets. Low-S/N single-pulse observations can lead to average single-pulse energies which lie below the receiver noise (thus, we see e.g. only noise and the log-normal tail of the brightest pulses), and may limit our ability to identify null pulses. The presence of null and multipeaked pulsars at high P_ℓ in Fig. 2 already indicate that multimodal pulsars may contaminate the log-normal sample. Unidentified nulling sources and low-signal measurements may potentially skew the log-normal parameter estimation, and we can see evidence of such an effect in an anticorrelation of low-$\langle s_\mathrm{E}\rangle$ pulsars with μ_ℓ in our data. To avoid contamination of our potential correlations by low-S/N data, we measured the σ_ℓ and μ_ℓ distributions only for pulsars whose single pulses were on average detected with significance $\langle s_\mathrm{E}\rangle > 4$. Figs 3 and 4 compare the probability distribution of the best-fitting σ_ℓ and μ_ℓ, respectively, of the $\langle s_\mathrm{E}\rangle > 4$ objects to the distributions of non-nulling and all objects. The non-nulling sources, although numbering only six, are completely unaffected by pulse nulling and provide a consistency check for the $\langle s_\mathrm{E}\rangle > 4$ distributions; a KS test between the non-nulling and $\langle s_\mathrm{E}\rangle > 4$ pulsars does not support the null hypothesis for σ_ℓ or μ_ℓ. The distribution of all sources is found to differ significantly from the $\langle s_\mathrm{E}\rangle > 4$ sources (supporting the null hypothesis at probabilities of 0.006 and <0.001 for σ_ℓ and μ_ℓ, respectively). This is not thought to be a physical effect, but as previously stated is likely to be caused by errors in parameter estimation in the low-signal sample due to the influence of noise or unidentified nulling. For comparison, we report the mean and standard deviation of σ_ℓ and μ_ℓ for the three populations in Table 2.

Only 3 per cent of our classifiable population were in agreement with a Gaussian distribution, of which only four objects (PSRs J0738−4042, J1507−4352, J1651−5222 and J1807−0847) had average single-pulse S/N of greater than 4. Of all the observed and derived physical properties tested (τ_c, B, P, $\dot{P}$, DM, pulse width and duty cycle), none stood out for these pulsars from the pulsars in the general population. Furthermore, they seem to share no characteristics in pulse shape or modulation, except that three of the four objects exhibit peaks in the R_j modulation parameter in the centre of the profile. However, this is not a characteristic that is unique to these objects. Both PSRs J0738−4042 and J1651−5222 exhibit intricate features in R_j, the former showing intensely modulated emission on the trailing pulse edge, and the latter appearing to exhibit two emission modes of similar energy, and possible subpulse drift. It is possible that these two objects have been misidentified as Gaussian, but in fact contain several profile modes whose mean energy properties share similar values.

Table 2. Average best-fitting log-normal parameters for three subsamples of the pulsars classified as log-normal or unimodal. Note that the $\langle s_\mathrm{E}\rangle > 4$ sources provide the fiducial sample values. Variance of the sample's values is given in parentheses.

Sample	N	$\langle\sigma_\ell\rangle$	$\langle\mu_\ell\rangle$
$\langle s_\mathrm{E}\rangle > 4$	19	0.11 (0.03)	1.18 (0.07)
Non-nulling	6	0.12 (0.03)	1.13 (0.04)
All	105	0.15 (0.07)	1.50 (0.42)

4.3 Multimodal energy distributions

A total of 18 pulsars in our sample had energy distributions classified as multimodal. It appears that the majority of these multimodal distributions are caused by mode changes; those with large relative energy peak differences exhibit mode changes that are visibly distinguishable in pulse stacks. We show two cases of this in Fig. 5, in which each pulsar exhibits two profile configurations that

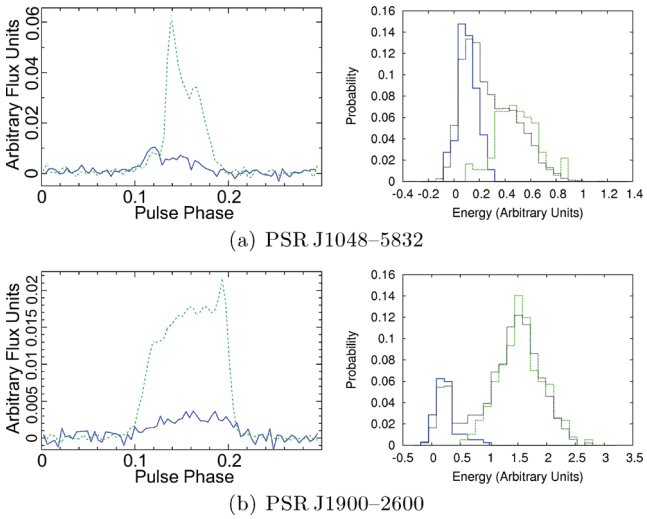

Figure 5. A view of the profile modes and their related energy distribution for two of our objects whose energy distributions were categorized as 'multipeaked'. In all panels, the dashed green, solid blue and dotted black lines correspond to the brighter mode, fainter mode and all combined pulses, respectively. The left-hand panels show the pulse profile integrated over a subset of pulses in each mode. The right-hand panels show a mode-divided energy analysis as well as the integrated analysis. In both cases, two modes account fully for the multiple peaks identified in the energy distribution, and the non-zero mean of the off-peak distribution is clear.

correspond to a change in observed energy.[4] It is likely that all multipeaked objects in our sample are the result of such profile reconfigurations, even if they are not always readily identifiable in our pulse stacks (e.g. due to faint emission and barely resolved profiles). For some pulsars, we cannot rule out that a transient component (e.g. giant bursts) on an otherwise steady profile is causing the second peak. We find it worthy of explicit mention that the inspection of energy distributions appears to be a straightforward way to identify mode changing in many pulsars, in which it might not be obvious from an inspection of only a pulse stack.

A clear ramification of the energy difference associated with mode changes is that some nulling pulsars may be exhibiting mode changes in which either the energy state drops below an observation's noise level (distinct from cessation of emission), or the beam configuration changes sufficiently such that no sub-beams are aimed at Earth. This has been previously suggested (e.g. Wang, Manchester & Johnston 2007; Timokhin 2010), and is supported by the faint emission seen in some pulsars after the integration of many 'null' pulses. For instance, PSR J1900−2600 (Fig. 5b) was previously identified as a nulling pulsar with a 10–20 per cent nulling fraction (Ritchings 1976; Mitra & Rankin 2008), which is approximately the fraction of pulses we observe in the low-energy mode. There are three contributions of our data to the 'nulls are mode changes' hypothesis: (1) mode changing appears to be fairly prolific (6 per cent of our whole sample had *discernible* multiple non-null energy peaks); (2) we observe a range of changes in mean integrated energy value, implying that some such pulsars could be misidentified as nulling or unimodal, thus the mode-changing population is probably larger; and (3) substantial reconfigurations may be more common than minor ones, given the 69 nulling pulsars and 18 multimodal objects in our sample. Three of our nulling pulsars exhibit multiple non-null peaks, thus may have multiple mode changes.

5 MODULATION STATISTICS OF PULSARS

Here, we discuss several distinct topics relating to pulse-to-pulse modulation in pulsars: Section 5.1 presents the modulation values across our full sample, characterizing the range of pulse-to-pulse modulation statistics of the general pulsar population. Section 5.2 discusses the phase-dependent location of modulation relative to the total intensity shape of the pulsar's profile in an attempt to understand if and how bursty (i.e. high-R_j) emission relates to the underlying pulsar beam shape. Finally, Section 5.3 describes correlation tests between the modulation parameters R and m with physical pulsar parameters.

In Table 1, we report three indicators of pulsar modulation: the maximum on-pulse R_j value, the minimum on-pulse m_j value and the S/N of the brightest single pulse detected in the blind single-pulse search, when these measurements are significant for a pulsar. We follow the significance threshold for m_j used by Weltevrede et al. (2006a) and Jenet & Gil (2003), in which the S/N of the integrated pulsar profile must be greater than 100. Because off-pulse values of R_j reflect the radiometer noise properties of the data, as previously noted, this statistic is only considered significant when the on-pulse peak R_j value is more than four times the standard deviation of R_j values in the off-pulse profile. Note that the maximum single-pulse search S/N should not necessarily correlate with m_j or R_j because they are calculated at a fixed time sampling, whereas the single-pulse search utilized a box-car search to fit for ideal pulse width.

5.1 Distribution of modulation parameters

The distribution of pulsars' minimum modulation index, m, provides a direct empirical snapshot of the pulsar population's typical modulation properties. Fig. 6 shows the distribution of m for our sample. While we do not distinguish various drift phenomena as in Weltevrede et al. (2006a), we can compare our results to theirs. In the Weltevrede et al. study, m was measured using a longitude-resolved power spectral technique rather than direct computation. While our distribution agrees in peak value, ours is moderately broader, and more heavily weighted towards higher m values than that of Weltevrede et al. This slight difference is possibly attributed to the difference in technique for mitigation of scintillation's contribution to m. While the Weltevrede et al. technique removed any low-frequency modulation (thus in addition to the $m_{\rm ISM}$ contribution, potentially removing some modulation attributable to the pulsar itself), our mitigation may have included an erroneous estimate of $m_{\rm ISM}$ due to errors in the Cordes & Lazio (2002) electron density distribution model. We would expect the former point to most strongly contribute to the observed effect.

In Fig. 7 we provide the R-parameter distribution. As previously noted and discussed further in Section 5.3, the R-parameter distribution cannot be taken at face value to be an 'intrinsic' modulation distribution due to its strong dependence on Gaussian statistics and mean single-pulse flux. However, note that a measured R_j value represents signal inconsistent with Gaussian variance; thus, these pulsars exhibit phase-resolved, sporadically varying emission. If (both integrated and phase-resolved) pulsar energy distributions are indeed log-normal, this result is not entirely unexpected. We note that in observations of increasing sensitivity, R_j values particularly of pulsars where the single-pulse mean is hiding in the noise (e.g.

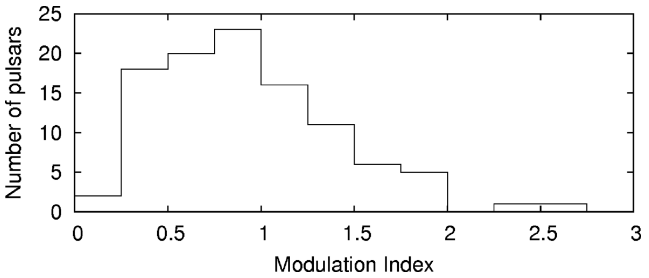

Figure 6. The distribution of minimum m_j value for the 103 pulsars with $S/N_{\rm int} \geq 100$, as discussed in Section 5.1.

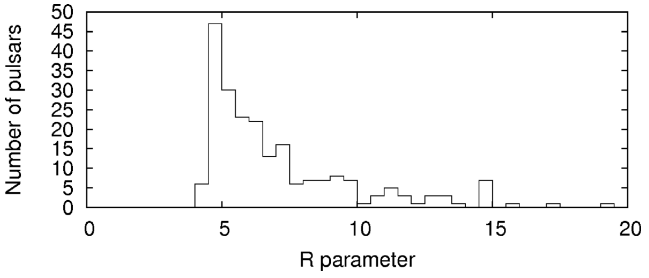

Figure 7. The distribution of maximum R_j value for the 222 pulsars for which this parameter was significant.

[4] By visual inspection of the energy distributions of the two modes, it appears there might also be a change in energy distribution statistics accompanying the mode change. This would have fascinating implications; however, we defer discussion on this until a more rigorous analysis can be performed.

deep nulling pulsars and RRATs) will increase. Additionally, the observed maximum R_j will scale with a sample's observing length, consistent with the probability distribution of emission energy. We thus expect that if the σ_ℓ and μ_ℓ values presented in Section 4.2 hold for the full population, the distribution shown in Fig. 7 would shift to higher values and perhaps broaden slightly, were our observing length and/or sensitivity increased.

5.2 Profile dependence of modulation

It has been noted in the literature that 'core' profiles (as defined by the profile classification scheme of Rankin 1983) are both less modulated than 'conal' profile components, and do not null. It has also been reported that giant pulse phenomena occur typically on the leading or trailing edge of pulsar profiles (certainly, the persistent modulation appears to be higher at pulse edges; m_j rises at the leading and trailing pulse edges for nearly the entirety of our sample). The R-parameter enables sensitivity to phase-resolved, sporadic emission behaviours. To explore the typical location of such emission and its relationship, if any, to integrated intensity profiles, we inspected each pulsar's total intensity and R_j profiles (sample R_j profiles are shown in Fig. 8, and all R_j profiles are shown in the online figures in the Supporting Information, Appendix A).

Persistent multiphase features in R_j appear to come in two types: broad, diffuse features that in many cases follow the rise and fall of the integrated intensity, and narrow features which have no pronounced counterpart in the total intensity profile thus presumably correspond to very sparse outbursts. The phase dependence of narrow R-parameter peaks varies vastly from pulsar to pulsar; however, in many objects, narrow R_j features appear on the edge of (leading or trailing) a *local* maximum in integrated intensity (not necessarily the brightest beam component). In some, the R_j profile is dual-peaked, with peaks falling on either side of the integrated profile. Examples of these are shown in Fig. 8. This is suggestive of a sporadic sub-beam-edge effect; however, as we do not have sufficient information to break down our profiles into conal or core components, we cannot say whether this effect is distinct to one profile geometry. Note, however, that in some pulsars the modulation does peak at the same phase as the integrated profile (in fact, PSR J1852−0636 as shown in Fig. 8d exhibits contemporaneously peaking modulation and intensity profiles for the outer sub-beams, but offset modulation peaks for the centre beam).

Finally, the variation of R_j values across a profile indicates an important point that will be discussed further in Sections 6.1 and 6.2, which is that the energy distribution (i.e. log-normal, power-law, Gaussian, etc. classification and distribution parameters) can be phase-dependent.

5.3 Correlation of modulation parameters with other neutron star parameters

We performed Kendall's τ correlation tests for the minimum m_j and maximum R_j against all basic pulsar physical parameters: age, magnetic field strength, energy loss rate, P, $\dot{P}$ and DM. We found no significant correlations that were not directly accountable by sample selection effects. m was found to correlate (in some cases, anticorrelate) with several parameters, most strongly with characteristic age and $\dot{E}$. However, we attribute all of those correlations to the strong anticorrelation between m and integrated S/N (Kendall's τ statistic: -0.55; probability $P_\tau < 0.000\,001$), which can induce correlations with m due to our fixed observation length (this 'correlation', as with the R-parameter/DM correlation below, is thought

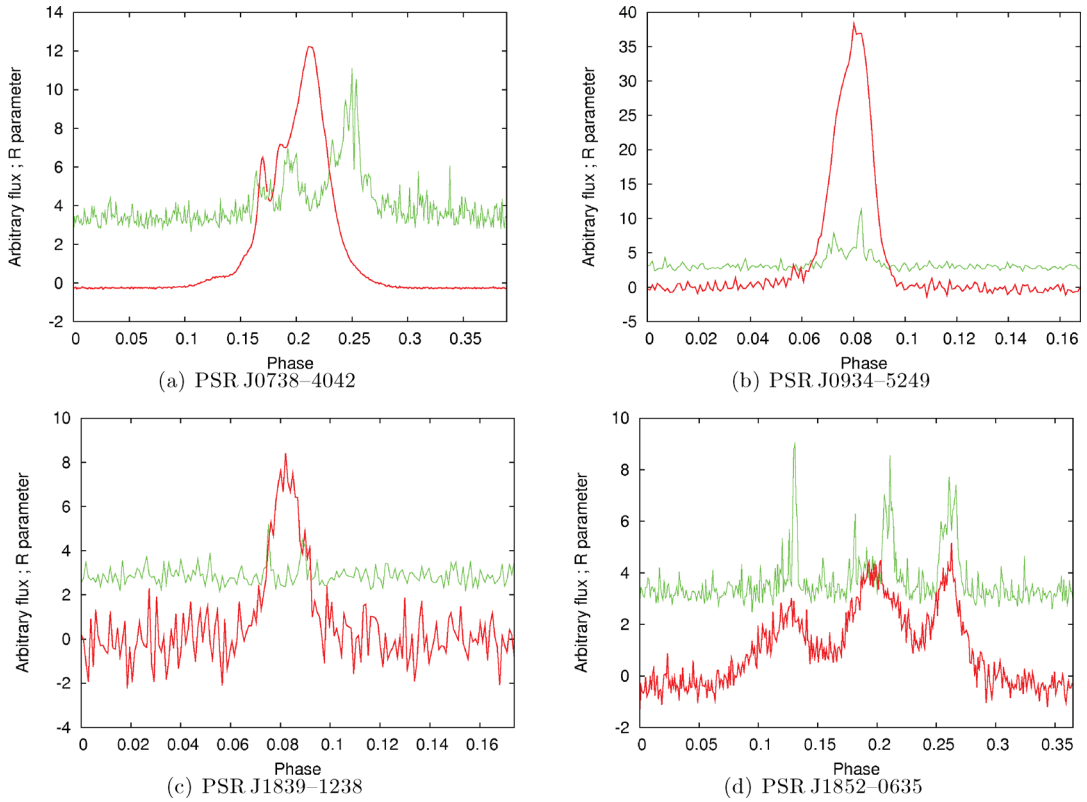

Figure 8. An expanded view of various R_j component profiles (thin green line) and their corresponding integrated intensity profile (thick red line). All of these profiles exhibit leading and/or trailing sporadic pulse components, primarily flanking local maxima in total intensity.

to be primarily the result of the low-weighted distribution of m and the few objects with strong integrated signal; the distribution of m at different signal intervals does not differ). The correlations were not significant when restricting the tests to pulsars with an integrated S/N between 100 and 400, indicating that these correlations were induced by the brightest ∼20 objects.

We measured no significant correlations between m_j and any of the complexity parameters of Jenet & Gil (2003), in agreement with Weltevrede et al. (2006a). Correlations between m and the complexity parameters are predicted to be stronger when considering m strictly from core pulse profiles (Jenet & Gil 2003); it is possible that if any correlations exist within these data, they are diluted by our lack of information about profile type and beam viewing angle. Potential errors in the NE2001 electron density model, leading to an incorrect treatment of scintillation's contribution to m, could also contribute to weakening a correlation. Thus, with the available information, our sample is unable to rule out any of the proposed theories with these correlation tests.

One correlation found with maximum R_j warrants brief discussion; the maximum R_j was weakly anticorrelated with DM ($\tau = -0.27$; $P_\tau < 0.000\,001$). We interpret this primarily as the naturally low-weighted distribution of maximum R_j (seen in the low-DM pulsars) and the fewer number of pulsars at high DM. However, pulse smearing and scattering may also dampen R-parameter values at high DM.

6 GENERAL DISCUSSIONS

Here we address three remaining points of discussion that arose from our analysis. Section 6.1 discusses physical motivators for the definition of the 'giant pulse' phenomenon in pulsars based on our energy distribution and pulse-to-pulse modulation measurements. We furthermore indicate how our analysis may indicate giant pulse activity occurring in several pulsars. Section 6.2 discusses the implication of our results for the net pulsar energy circuit, paying particular attention to a discrepancy between the narrow range in integrated single-pulse energy values versus the large range in phase-resolved bursty emission. We also draw on the results of interpulse pulsars in this discussion. Finally, in Section 6.3, we point out peculiar behaviours observed in several pulsars that were identified in the course of our analysis.

6.1 Giant pulses versus log-normal pulses

The definition of 'giant pulse' has varied in previous analyses, with some authors defining the term as any pulse with a flux more than 10 times the average flux at that phase, and others differentiating giant pulses by their power-law energy distributions. In our analysis, the former definition translates directly to the specification $R > 10$. This condition is not uncommon in this data set, and furthermore the R-parameter's continuous distribution over a broad range indicates that this differentiation of 'giant pulse' is entirely arbitrary. While it is certainly a convenient definition, if many pulsars are indeed log-normally distributed, no physical distinction (except for small variations in σ_ℓ) should exist between high- and low-R_j pulsars. We therefore support the latter definition of 'giant pulse', which in addition denotes a clear difference in underlying plasma processes.

As we have previously noted, a significant measurement of R_j implies the presence of non-Gaussian statistics in phase bin j, and does not strictly differentiate between what non-Gaussian distribution is causing the heightened R_j. For the pulsars with significantly measured R_j values, we have an insufficient number of pulses in our data to perform an assessment of whether the phase-resolved energy distributions are caused by a pure log-normal distribution, or by the log-normal plus power-law tail that is exhibited at giant-pulsing phases in some pulsars. However, studies of these high-R-parameter objects over a longer time-scale could provide the data necessary to differentiate pulsars with broad phase-resolved log-normal distributions from power-law-distributed giant pulses as the cause of the intense modulation (see e.g. Karuppusamy, Stappers & Serylak 2011).

Although the broad time resolution used in our observations would dampen the intensity and prominence of giant micropulses, we can check for an indication of such activity by inspecting the data for very narrow (i.e. unresolved in phase) significant features in R_j. Several pulsars show clear potential signs of such an effect: PSRs J0726−2612, J1047−6709 (the small, narrow feature preceding the main pulse), J1759−1956 and J1801−2920 (see Appendix A).

6.2 Energy budgets and additional insight from interpulse pulsars

We find it striking that for $\langle s_E \rangle > 4$ pulsars, the maximum deviation of integrated pulse energy from $E/\langle E \rangle$ tends to be fairly low. Inspecting the maximum integrated energy deviation (M_E) in these pulsars, we find that they lie in the range $1.6 < M_E < 6.4$, with a mean of 2.9; that is, the integrated pulse energy tends to not deviate vastly from its mean value. One might expect maximum R_j to correlate with M_E, given the excess energy one would expect to be provided by a bright, phase-resolved pulse. In Fig. 9, we show a scatter plot of maximum R_j versus M_E for pulsars with $\langle s_E \rangle > 4$ and a significantly measured R_j value. While there is a weak correlation here (Kendall's τ test gives $\tau = 0.29$, $P_\tau = 0.001$), the scatter in both variables is significant.

This scatter and the fact that R_j for some pulsars is large across a broad phase range indicates that many phases may be emitting large bursts of energy; as previously noted, phase-resolved changes in R_j indicate the possibility that the energy distribution is likewise phase-dependent. Despite this, however, we see only a small range of M_E values, and at least 45 per cent of our sample has an integrated pulse energy distribution that is well fitted to a unimodal (mostly log-normal) distribution. What this appears to imply is that despite the occurrence of sizeable sub-beam variations, a large outburst at one phase is compensated by a deficit of or weakened emission at other phases, such that a narrow integrated distribution in energy may be

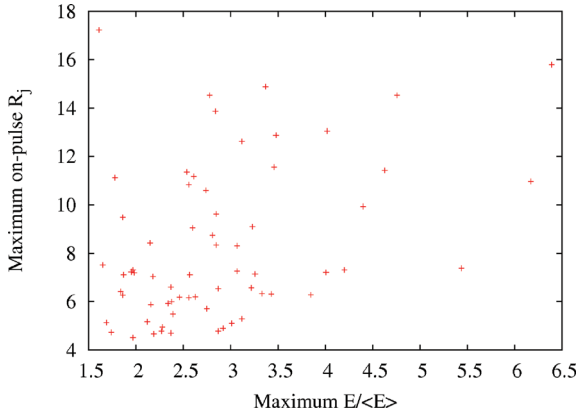

Figure 9. The R-parameter plotted against the maximum deviation of integrated normalized pulse energy.

maintained. Thus, there appears to be a self-balancing effect, i.e. there is a net energy regulation by which the total sub-beam circuit is governed.

Similarly, previous studies have indicated that pulsars with interpulses show a relationship in the pulses' emission properties. Various studies have shown correlations or anticorrelations in the amplitude of main pulses and interpulses (e.g. Fowler & Wright 1982; Biggs 1990). Furthermore, Weltevrede et al. (2006a) found the same periodicity of amplitude modulation in the main/interpulse of PSR J1705−1906.

We identified five interpulse pulsars in our sample; the main and interpulses for these pulsars ('interpulse' here being the fainter component) have separately reported statistics in Table 1, marked by (m) and (i), respectively, in addition to the statistics from the total integrated emission window. We find agreement between maximum R_j in the main pulse and interpulse only in the case of PSR J1705−1906, which despite a factor of ∼7 difference in emission intensity, the maximum R_j values both peak from 8 to 10. This is particularly notable as it supports the aforementioned findings of Weltevrede et al. (2006a, 2007).

In the other interpulse pulsars, all but PSR J0908−4913 exhibit R_j values significant only in the main pulse. We note that even in the presence of a pulsar-wide energy regulation, these discrepancies may not be surprising given the strong phase dependence of R_j and thus its implied dependence on viewing angle. Accordingly, it may be that we view PSR J1705−1906's main pulse and interpulse at an angle such that we see corresponding primary and counter-beam components; while the other pulsars might share properties between particular sub-beams, their properties could be masked by an unfavourable viewing angle.

The energy distribution classification differences between main pulse, interpulse and net emission are also interesting to consider in this discussion. However, due to the low $\langle s_E \rangle$ on all of the interpulses, the data do not provide clear results on this topic. Most of the classifications are 'other', and only the interpulses of PSR J1705−1906, J1739−2903 and J1825−0935 are well fitted to a log-normal distribution. While this seems to imply that the main pulse and interpulse energy distributions do not share the same underlying plasma statistics, higher S/N measurements would be more suitable to explore the relationship between the main/interpulse integrated energy distribution.

6.3 Notes on anomalous pulsar properties

In our online figure (see Appendix A), we display the pulse stack, modulation and intensity profiles, and energy distribution with fits for each pulsar. These graphics provide a wealth of information, and upon viewing them, nearly every pulsar appears to have some unique and fascinating feature. As such, the plots contain far more features of interest than are relevant for the discussion in this paper. The reader is encouraged to inspect the data and pursue outstanding features that catch their interest. Examples of peculiar behaviour which stood out to us are: the cyclic, phase-dependent nulling of PSR J1133−6250, the atypically broad energy distributions of PSRs J1243−6423, J1047−6709, J1401−6357, J1456−6843 and J1745−3040, and the ordered beating visible in the pulse stack of PSR J1534−5334.

Below, we do describe unconventional emission discovered in several pulsars, for cases where the anomalous behaviour is not recognizable from the displayed data.

6.3.1 Multistate nulling fraction pulsars

Burke-Spolaor & Bailes (2010) reported what appeared to be a 'part-time RRAT', PSR J0941−39, which at times is observable as a nulling pulsar with a null fraction of ∼10 per cent, and at other times emits single pulses at a rate of ∼2 per minute. Our analysis has identified several potential further examples of these. The first is PSR J0828−3417, which was originally noted to have low-level emission during its 'nulls' by Esamdin et al. (2005). We note that in fact their 'low-level emission' appears to be made up of sporadic single pulses, similar to PSR J0941−39. We furthermore discovered one pulse from PSR J1107−5907, which has been previously reported as an 'intermittent pulsar' whose emission alternates between states of bright, weak and null emission on a yet-unknown time-scale (Kramer 2008; O'Brien 2010). Archival data from this pulsar also reveal erratic changes in nulling fraction, particularly directly preceding its constant on state. We think it pertinent to point out that each of these pulsars exhibit changes not only in intensity (i.e. nulls or mode changes when emission appears to cease), but also in the *relative time spent* in on and off configurations.

6.3.2 Wide nulling distribution of PSR J1255−6131

We detected only one pulse from PSR J1255−6131, and no integrated emission. The single pulse was of high significance (S/N ∼ 10), and thus given the apparently large nulling fraction, we were motivated to explore archival data for this pulsar. We found ∼20 archival pulse stacks at a central frequency of 1.4 GHz. These observations were collected as follow-up to the Parkes multibeam survey, and the data format and observing system is as described in the survey's paper (Manchester et al. 2001). The data available to us were each of length 5–30 min, formed into pulse stacks and often averaged over 1-min intervals so we could not probe single-pulse behaviour. We found that PSR J1255−6131 displayed a great range of activity cycle times in these observations. Occasionally the pulsar appeared to emit without ceasing over lengths of 5–10 min; however, more commonly it exhibited bursts of emission lasting up to 3 min. The null fraction from observation to observation ranged between 10 and 100 per cent. We estimate that the null fraction for the pulsar is typically around 70–80 per cent; however, with a broad emission cycle range. This pulsar may be exhibiting a variation of the null-change behaviour discussed in the above section. However, the behaviour in this pulsar differs as its nulling fraction distribution does not appear to be bimodal, but rather is an unusually broad, and may be either stochastic, or a smoothly distributed function. The HTRU med-lat survey pointing appears to have caught PSR J1255−6131 at the sparsest tail of this null fraction distribution.

6.3.3 Off-pulse emission and PSR J1406−5806

The careful cleaning of interference in our data enabled us sensitivity to short-duration, off-pulse emission (i.e. emission more than 5 per cent in phase from integrated profile components). We found such emission in only one pulsar, PSR J1406−5806. Pulses were detected across the full phase range, though its 'on-pulse' emission appears also to be highly sporadic. Upon stacking all available archival pulse stacks from Parkes telescope (3 h total), the off-pulse emission contributes weak components to a stable integrated profile. We interpret this object as an aligned rotator with a high nulling fraction. The lack of off-pulse emission in other pulsars indicates

no evidence that the emission detected by Basu, Athreya & Mitra (2011) is made up of sporadic, bursty emission.

7 SUMMARY AND CONCLUSIONS

We analysed the pulse-to-pulse energy and modulation properties of all pulsars serendipitously observed in the HTRU med-lat survey to emit detectable single pulses. This sample was derived from the 702 pulsars redetected by the HTRU med-lat observations, yielding this survey a single-pulse detection rate of 45 per cent. 16 of these pulsars were only detected through the single-pulse search.

For our full 315-pulsar sample, we performed energy distribution fits to determine the suitability of log-normal or Gaussian distributions to describe integrated pulse-to-pulse energy. This analysis showed that more than 40 per cent of our sample fits a log-normal pulse energy distribution, while only a few pulsars were well fitted to a Gaussian distribution. Other pulsars were not fitted by either distribution; however, this may be due to (a) the influence of noise on a faint pulsar, (b) unrecognized nulling/mode changing, or (c) a non-Gaussian, non-log-normal underlying energy distribution. Because of the large likelihood of (a) and (b) to disrupt our fits, we suggest that a greater fraction of pulsars may show unimodal and log-normal pulse energy distributions; however, observations of higher sensitivity and a greater number of detected pulses will be required to address this.

Some pulsars were found to have bimodal or multimodal energy distributions, which we demonstrated to be caused by mode changes in some pulsars. Energy distribution inspection can thus be useful for identifying mode changes where they might not be obvious in a pulse stack. Multi-energy states have implications for nulling pulsars, supporting the argument of Timokhin (2010) that some pulsars observed to 'null' may simply be reconfigured into a state where fainter, fewer or no sub-beams are directed at the observer. Along these lines, we demonstrated that the previously 'nulling pulsar' PSR J1900−2600 exhibits faint emission in its low state. It should be noted that for some multimodal-energy pulsars, particularly those with short-change time-scales or those with minimal differences in mode energies, we cannot distinguish between mode changing and other longitude-resolved modulation (e.g. a distinct transient sub-beam).

Mode-changing properties are not to be confused with another state-change effect observed in only a few pulsars. PSRs J0828−3417 and J1107−5907 appear to have two discrete nulling fraction states; as with PSR J0941−39 (Burke-Spolaor & Bailes 2010), these objects switch between being pulsars with null fraction <10 per cent, to a separate state where they sporadically emit single pulses per many rotations. The single-pulse state may have previously been falsely identified as a low-energy mode change (Esamdin et al. 2005; O'Brien 2010), as during long integrations bright single pulses are dampened by the addition of null rotations.

We reported longitude-resolved modulation statistics, quantified by the modulation index m and the R-parameter, the latter used to identify non-Gaussian sporadic emission. We found no correlations between m or R and physical parameters (e.g. age, spin-down energy) or the complexity parameters predicted by various energy models.

We found that outbursts with distribution significantly deviating from Gaussianity *can* occur across a pulsar's full integrated profile; however, occasionally this modulation intensifies at the rising and/or falling edge of components in the integrated profile. This may indicate a conal or core edge modulation effect, and/or the presence of giant pulses at the corresponding pulse phase. Our analysis supports the fact that physically distinctive 'giant pulse' phenomena should be defined because they have power-law statistics; however, we have insufficient data to assess the shape of high-energy tails in our high-R-parameter pulsars.

Finally, in considering the large phase-resolved deviations seen in the R_j profiles of some pulsars in conjunction with the distribution of integrated single-pulse energy in these pulsars, it is striking that the energy typically deviates only up to three times its average value. This is suggestive of a beam-wide energy regulation that affects all angles of the pulsar's beam, and we broaden our consideration of this possibility using information from interpulse statistics. Only one of our five interpulse pulsars exhibits a notable relationship in modulation properties between the main and interpulse; however, we cannot make conclusive statements about the main/interpulse energy distribution relationship due to the low signal from the interpulses in these pulsars.

ACKNOWLEDGMENTS

The Parkes radio telescope is part of the Australia Telescope National Facility which is funded by the Commonwealth of Australia for operation as a National Facility managed by CSIRO. A portion of research was carried out at the Jet Propulsion Laboratory, California Institute of Technology, under contract with the National Aeronautics and Space Administration.

REFERENCES

Backer D. C., 1970, Nat, 228, 42
Basu R., Athreya R., Mitra D., 2011, ApJ, 728, 157
Biggs J. D., 1990, MNRAS, 246, 341
Biggs J. D., 1992, ApJ, 394, 574
Burke-Spolaor S., Bailes M., 2010, MNRAS, 402, 855
Burke-Spolaor S. et al., 2011, 416, 2465
Cairns I. H., Johnston S., Das P., 2001, ApJ, 563, L65
Cairns I. H., Johnston S., Das P., 2003a, MNRAS, 343, 512
Cairns I. H., Das P., Robinson P. A., Johnston S., 2003b, MNRAS, 343, 523
Cairns I. H., Johnston S., Das P., 2004, MNRAS, 353, 270
Cognard I., Shrauner J. A., Taylor J. H., Thorsett S. E., 1996, ApJ, 457, L81
Cole T. W., 1970, Nat, 227, 788
Comella J. M., Craft H. D., Lovelace R. V. E., Sutton J. M., 1969, Nat, 221, 453
Cordes J. M., Lazio T. J. W., 2002, Astrophysics e-prints arXiv:astro-ph/0207156
Esamdin A., Lyne A. G., Graham-Smith F., Kramer M., Manchester R. N., Wu X., 2005, MNRAS, 356, 59
Fowler L. A., Wright G. A. E., 1982, A&A, 109, 279
Jenet F. A., Gil J., 2003, ApJ, 596, L215
Johnston S., Romani R. W., 2002, MNRAS, 332, 109
Johnston S., Romani R. W., 2003, ApJ, 590, L95
Johnston S., van Straten W., Kramer M., Bailes M., 2001, ApJ, 549, L101
Karuppusamy R., Stappers B. W., Serylak M., 2011, A&A, 525, A55
Keane E. F., Kramer M., 2008, MNRAS, 391, 2009
Keith M. J. et al., 2010, MNRAS, 409, 619
Kramer M., 2008, in Bassa C., Wang Z., Cumming A., Kaspi V. M., eds, AIP Conf. Ser. Vol. 983, 40 Years of Pulsars: Millisecond Pulsars, Magnetars and More. Am. Inst. Phys., New York, p. 11
Kramer M., Johnston S., van Straten W., 2002, MNRAS, 334, 523
Levin L. et al., 2010, ApJ, 721, L33
Lundgren S. C., Cordes J. M., Ulmer M., Matz S. M., Lomatch S., Foster R. S., Hankins T., 1995, ApJ, 453, 433
McLaughlin M. A., Cordes J. M., 2003, ApJ, 596, 982
McLaughlin M. A. et al., 2006, Nat, 439, 817
Manchester R. N. et al., 2001, MNRAS, 328, 17
Manchester R. N., Hobbs G. B., Teoh A., Hobbs M., 2005, AJ, 129, 1993

Miller J., McLaughlin M., Rea N., Keane E., Lyne A., Kramer M., Manchester R., Lazaridis K., 2011, in Burgay M., D'Amico N., Esposito P., Pellizzoni A., Possenti A., eds, AIP Conf. Ser. Vol. 1357, Radio Pulsars: An Astrophysical Key to Unlock the Secrets of the Universe. Am. Inst. Phys., New York, p. 161
Mitra D., Rankin J. M., 2008, MNRAS, 385, 606
O'Brien J., 2010, PhD thesis, Univ. Manchester
Rankin J. M., 1983, ApJ, 274, 333
Ritchings R. T., 1976, MNRAS, 176, 249
Staelin D. H., Reifenstein E. C., III, 1968, Sci, 162, 1481
Timokhin A. N., 2010, MNRAS, 408, L41
Wang N., Manchester R. N., Johnston S., 2007, MNRAS, 377, 1383
Weisberg J. M., Armstrong B. K., Backus P. R., Cordes J. M., Boriakoff V., Ferguson D. C., 1986, AJ, 92, 621
Weltevrede P., Edwards R. T., Stappers B. W., 2006a, A&A, 445, 243
Weltevrede P., Stappers B. W., Rankin J. M., Wright G. A. E., 2006b, ApJ, 645, L149
Weltevrede P., Stappers B. W., Edwards R. T., 2007, A&A, 469, 607

APPENDIX A: DATA VIEWGRAPHS

Detailed data viewgraphs for each of the 315 pulsars in our sample are provided as Supporting Information with the online version of the paper. An example is shown in Fig. A1.

SUPPORTING INFORMATION

Additional Supporting Information may be found in the online version of this article.

Appendix A. Data viewgraphs for each of the 315 pulsars in our sample.

Please note: Wiley-Blackwell are not responsible for the content or functionality of any supporting materials supplied by the authors. Any queries (other than missing material) should be directed to the corresponding author for the article.

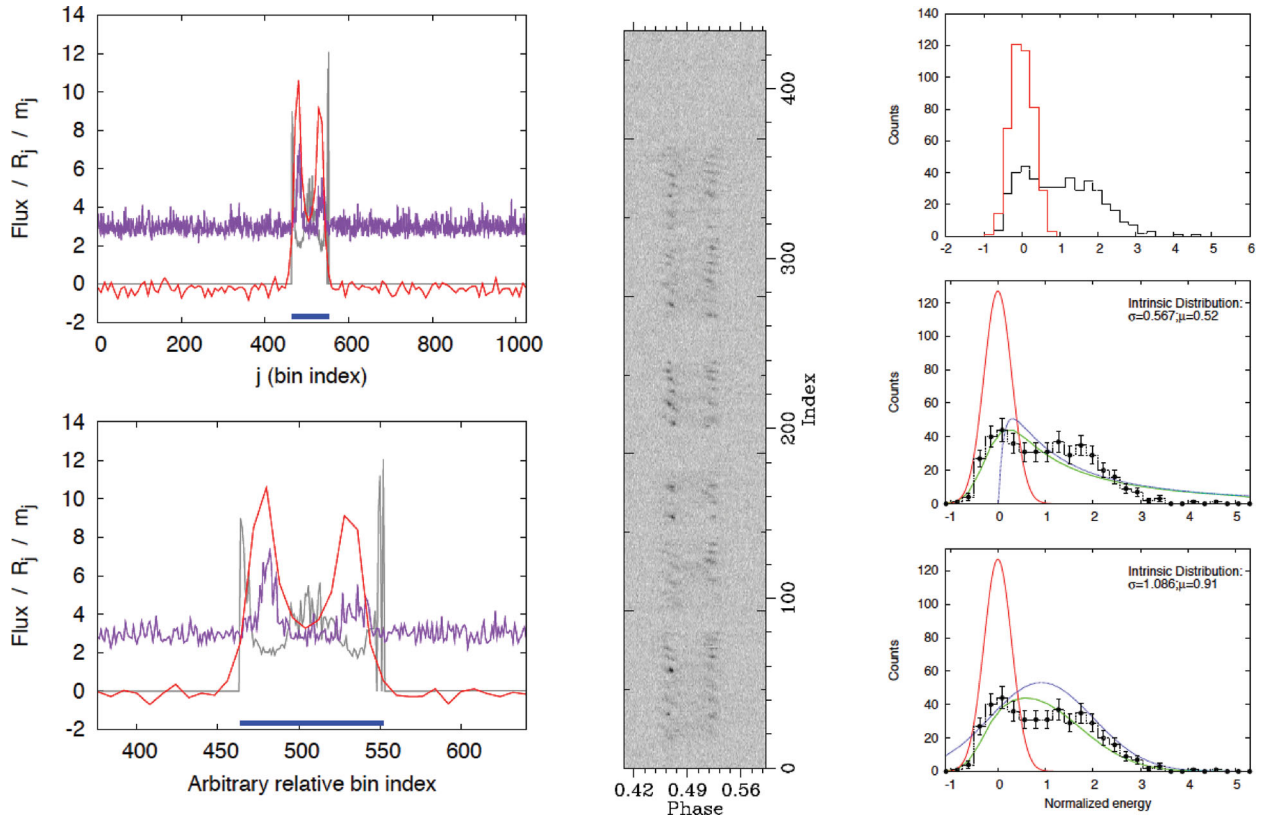

Figure A1. One example of a plot from the online Supporting Information. These panels show the data corresponding to pulsar PSR J1727−2739. In addition to the figures shown here, the Supporting Information also provides the pulsar's J2000 name, DM and period, and the observation's start time in Universal Coordinated Time for reference. See the text for panel descriptions.

This paper has been typeset from a TEX/LATEX file prepared by the author.